Cosmogenic nuclide techniques

Joerg M. Schaefer[1,8]✉, Alexandru T. Codilean[2,3], Jane K. Willenbring[4,8], Zheng-Tian Lu[5], Benjamin Keisling[1], Réka-H. Fülöp[2,6] and Pedro Val[7]

Abstract | Cosmogenic nuclide techniques have advanced the geosciences by providing tools for exposure age dating, burial dating, quantification of denudation rates and more. Advances in geochemistry, accelerator mass spectrometry and atom trap trace analyses are ushering in a new cosmogenic nuclide era, by improving the sensitivity of measurements to ultra-trace levels that now allow new applications of these techniques to numerous Earth surface processes. The advances in cosmogenic nuclide techniques have equipped the next generation of geoscientists with invaluable tools for understanding the planet, but addressing pressing needs requires rising to an even greater challenge: imbuing within the cosmogenic community, and the geosciences as a whole, a commitment to justice, equity, diversity and inclusion that matches our dedication to scientific research. In this Primer, we review the state of the art and recent exciting breakthroughs in the use of cosmogenic nuclide techniques, focusing on erosion factories over space and time, and new perspectives on ice sheet stability. We also highlight promising ways forward in enhancing inclusion in the field, as well as obstacles that remain to be overcome.

Rates of production
The rates at which specific nuclides are produced from a specific element or in a mineral. Production rates for all terrestrial cosmogenic nuclides vary spatially and appear to have varied temporally; they are often reported as normalized to sea level and high latitude.

Cosmogenic accumulation clock
Cosmic ray neutrons and muons produce terrestrial cosmogenic nuclides in near-surface rocks as a function of time.

Cosmogenic decay clock
Terrestrial cosmogenic nuclides in buried rocks decay according to their half-lives or remain constant if the cosmogenic nuclides are stable.

✉e-mail: schaefer@ldeo.columbia.edu

https://doi.org/10.1038/s43586-022-00096-9

Dedicated to Didier Bourlès (1955–2021).

Methods relying on cosmogenic nuclides have transformed geosciences since the 1950s (REFS[1–15]). Cosmogenic nuclides are produced when surface rocks are exposed to the open sky and bombarded by cosmic rays. Primary cosmic radiation, mostly protons born in supernovae in space, hit the Earth's upper atmosphere and go through a cascade of particle reactions. These reactions create secondary cosmic rays, mostly neutrons and muons, that finally reach the Earth's surface (FIG. 1A,B). Those cosmic neutrons and muons interact with target atoms in near-surface minerals, including oxygen, silicon, potassium, calcium and iron, and produce terrestrial cosmogenic nuclides (TABLE 1). The rates of production of these nuclides are now relatively well known[16,17], as are the half-lives of the radioactive cosmogenic nuclides, and so measuring their concentration in samples and accounting for production rates and half-lives of the nuclides allows us to estimate the age of the sample.

Cosmogenic nuclide methods provide direct, quantitative information about the three general Earth surface processes influencing the cosmogenic nuclide inventory of surface rocks and sediments. The first is by providing information about exposure to the open sky, and thus cosmic rays, when the cosmogenic accumulation clock is ticking and all cosmogenic nuclides are produced in situ as a function of time according to their respective production rates. The second is the burial of a previously exposed surface, shielding the surface from cosmogenic production, when the cosmogenic decay clock starts ticking, and cosmogenic nuclide ratios change with the burial time as a function of one single parameter, the difference in the half-lives of the cosmogenic nuclides. Finally, denudation of surfaces exposed to cosmic rays via physical erosion and chemical weathering causes exhumation of previously shielded material from depth to the surface, followed by fluvial or alluvial transport to a depocentre where sediment is buried — locking in a cosmogenic nuclide record of its arduous path.

The most straightforward and most widely used application of cosmogenic nuclides in geosciences is referred to as surface exposure dating (FIG. 1), which makes use of the production of cosmogenic nuclides and their accumulation in a rock surface as a function of time since the surface was initially exposed. The measured cosmogenic nuclide concentration (atoms per gram of target mineral) in the sample divided by the production rate (atoms per gram per year) yields the exposure age (years).

Cosmogenic nuclide burial dating[18] uses the different rates of radioactive decay of multiple cosmogenic nuclides co-produced in a rock to determine the length of time that a previously exposed surface has been buried, and thus shielded from cosmogenic nuclide production. The most frequently used nuclide system is the $^{26}Al/^{10}Be$ pair co-produced in quartz. The production rate of ^{26}Al is about seven times that of ^{10}Be in quartz[19–21] (6.7–7.3 is the currently discussed range of this production ratio). If this surface is buried — by a landslide or a readvancing ice sheet, for example — and cosmogenic

Author addresses

[1]Lamont–Doherty Earth Observatory, Columbia University, Palisades, NY, USA.
[2]School of Earth, Atmospheric and Life Sciences, University of Wollongong, Wollongong, New South Wales, Australia.
[3]ARC Centre of Excellence for Australian Biodiversity and Heritage (CABAH), University of Wollongong, Wollongong, New South Wales, Australia.
[4]Department of Geological Sciences, Stanford University, Stanford, CA, USA.
[5]School of Physical Sciences, University of Science and Technology of China, Hefei, Anhui, China.
[6]NST - The Environment, Australian Nuclear Science and Technology Organisation (ANSTO), Lucas Heights, New South Wales, Australia.
[7]Department of Geology, Federal University of Ouro Preto, Ouro Preto, Minas Gerais CEP, Brazil.
[8]These authors contributed equally: Joerg M. Schaefer, Jane K. Willenbring.

production stops, the ^{26}Al/^{10}Be ratio changes according to the difference in decay rates between the shorter-lived ^{26}Al (half-life of ~705 kyr (REF.[22])) and the longer-lived ^{10}Be (half-life of 1.4 Myr (REFS[23,24])).

A third general field of cosmogenic nuclides in geoscience is the quantitative evaluation of the rate of denudation by physical erosion and chemical weathering[5,25]. The residence time of rock and soil through the upper metres of the Earth's surface is recorded by the concentrations of cosmogenic nuclides measured in minerals or on minerals (FIG. 1), with slowly eroding surfaces having sufficient time to build up large quantities of cosmogenic nuclides, and surfaces quickly exhumed from depth replaced by new fresh material with low or negligible concentrations. Denudation measured via meteoric ^{10}Be has been a topic of renewed attention in the past decade[26,27], but we do not focus on this application here. Unlike meteoric ^{10}Be that is subject to grain-scale, surface-adsorption processes governed by soil biogeochemistry and aqueous reactive transport, cosmogenic nuclides produced in situ in minerals of surface rocks serve as quasi-conservative tracers. Their unique, depth-dependent production and loss via strict laws of radioactive decay and denudation provide quantitative means of monitoring processes in which there is a vertical component to the movement of material relative to the surface, such as erosion of mountain peaks, production of soil or erosion integrated over a wider area, such as an amalgamation of sand grains from a river mouth. The latter has been particularly prominent over the past decade both in actively eroding landscapes and in sediment archives, which, when dated, can provide records of how landscapes have evolved over time[28,29].

Denudation
The process of erosion, leaching and stripping due to the removal of material from higher to lower areas. The sum of weathering and erosion.

Surface exposure dating
Sampling a surface after an exposure time *t* and measuring the cosmogenic nuclides on the surface, divided by the production rate of this nuclide at this location and during this exposure time.

Burial dating
Buried samples measured after a burial time, where the terrestrial cosmogenic nuclide ratios reflect the period of burial and constrain the duration.

Cosmogenic nuclides produced in the atmosphere such as meteoric ^{10}Be (REF.[30]), ^{81}Kr (REF.[31]) and ^{39}Ar (REF.[32]) have been widely useful. Meteoric ^{10}Be records provide critical information about the atmospheric ^{10}Be production influenced by solar, geomagnetic and meteorologic variations[30], as well as geomorphic and marine changes. The advent of an entirely new measurement technique for cosmogenic nuclides, the atom trap trace analysis (ATTA) technique[33], now allows dating of ancient groundwaters and ice with ^{81}Kr (REFS[34,35]), and to apply ^{39}Ar to tackle important questions about the global ocean circulation[33,36].

Beyond summarizing the major cosmogenic nuclide applications and the underlying techniques, this Primer discusses two forefront areas of cosmogenic nuclide geosciences: multi-cosmogenic nuclide techniques to directly measure/map the instability of the Greenland Ice Sheet during past warm periods and to date the oldest ice in Greenland, which are still in the pioneering phase and already impact climate science and geosciences; and cosmogenic nuclide constraints on the erosion of landscapes and how topography changes as a function of climate, tectonics and life. Further, we present what we perceive as the cutting edge of the established cosmogenic nuclide techniques in geosciences, discussing the current limitations in reproducibility and inter-comparability between projects and reporting improvement potential. Finally, we present an outlook for the next 10 years and make predictions for where the biggest impacts and transformations might occur. In closing, we present recommendations for ushering the cosmogenic nuclide geosciences community into a new era defined by increased attention to justice, equity, diversity and inclusion, to make the field welcoming and safe for everyone wishing to participate.

Experimentation

Cosmogenic nuclide applications in geoscience rely on the measurements of minute amounts of cosmogenic nuclides in a wide variety of natural samples, including surface rocks, terrestrial sediments, river sediments, ocean sediments, snow, rain, ice, ocean water and meteorites. Recently, cosmogenic nuclide measurements were reported from trees[37]. A thorough review of the wide variety of samples and the complex process of sample selection and sampling techniques for cosmogenic nuclide analyses far exceeds the scope of this Primer; sampling concepts and challenges can be found elsewhere[11,38].

Cutting-edge measurements of cosmogenic nuclides from different samples require the synergetic interplay between complex geochemical and analytical methods. For example, to measure cosmogenic nuclides from surface rocks, high-purity mineral separates have to be produced from the whole rock, ranging from tens of milligrams to 50–100 g in mass. Only certain mineral phases are suitable for specific cosmogenic nuclide analyses — such as quartz for ^{10}Be, ^{26}Al, ^{14}C and ^{21}Ne, pyroxene and olivine for ^{3}He and ^{21}Ne, and feldspar and pyroxene for ^{36}Cl; these mineral phases are ubiquitous in Earth surface rocks, allowing for widespread application of cosmogenic nuclide techniques. Analysis of the respective cosmogenic isotopes is performed by complex and high-end machines such as accelerator mass spectrometers[2] and noble gas mass spectrometers[39], and, as of very recently, by ATTA. FIGURES 2 and 3 present an overview of the geochemistry and analytics involved in modern cosmogenic nuclide measurements. In this section, we discuss specific experimental aspects and novelties, focusing on the most widely used cosmogenic nuclides, including the cosmogenic workhorses ^{10}Be and ^{26}Al, the recently refined and versatile ^{36}Cl, the fast-decaying ^{14}C co-produced with ^{10}Be, ^{26}Al and ^{21}Ne in quartz and the stable cosmogenic noble gases ^{3}He and ^{21}Ne. Beyond, we include here the cutting-edge experimental techniques that now enable measurement of the

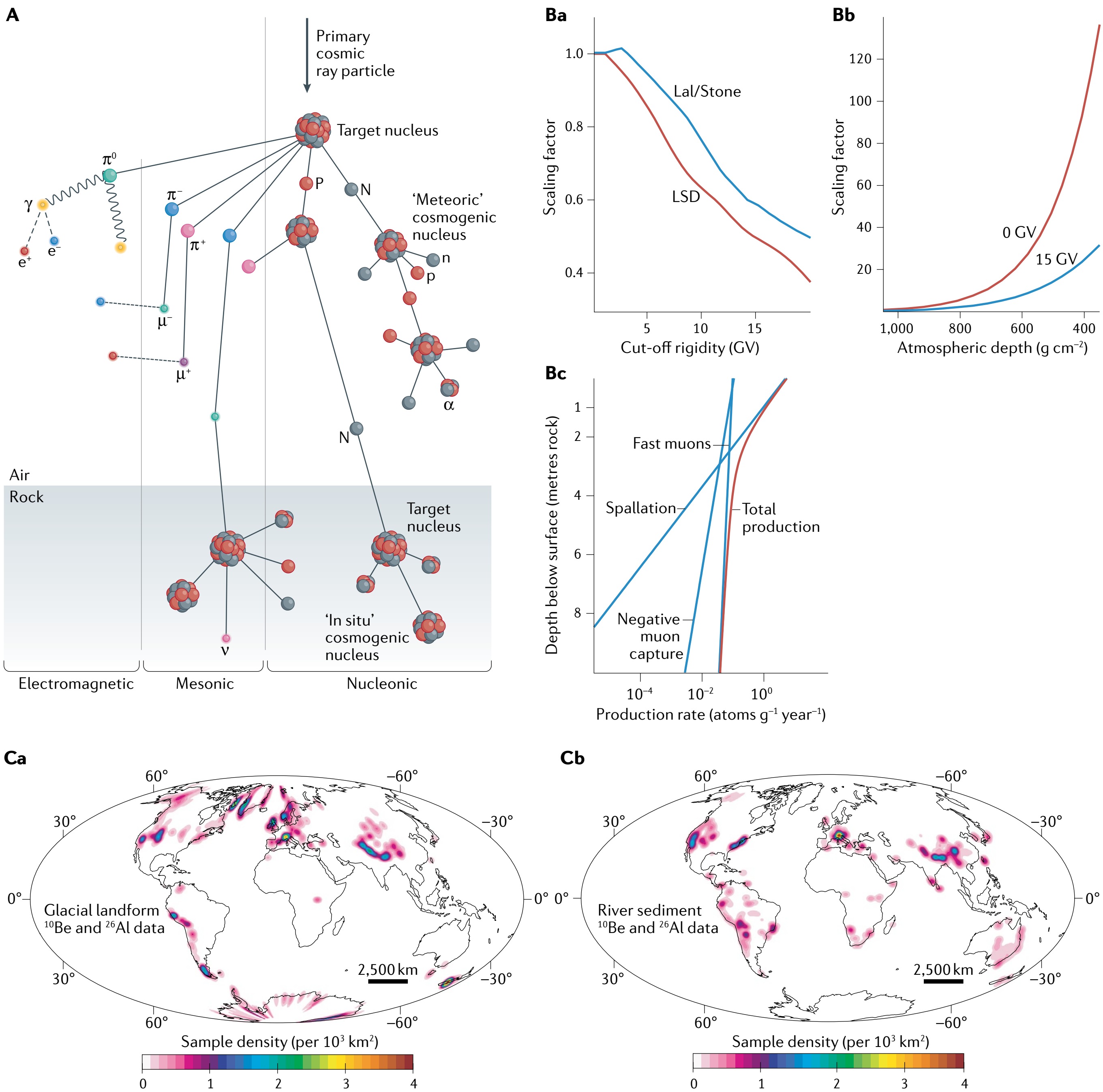

Fig. 1 | **Cosmogenic nuclide production systematics. A** | Primary cosmic ray particles (mostly protons) enter top of the atmosphere and produce a cascade of heavy (nucleonic) and lighter (mesonic) particles and electromagnetic showers. This nuclear cascade results in production of cosmogenic nuclides in the atmosphere (termed meteoric) and in rocks making up the surface of the Earth (termed in situ). P, N, high-energy (>10 MeV) secondary protons and neutrons cascading to the Earth's surface; n, p, α, secondary particles not cascading to the Earth's surface; π^+/π^-, μ^+/μ^-, ν, e^+, e^-, γ, pions, muons, neutrinos, positrons, electrons and gamma rays. **B** | In situ cosmogenic nuclide production latitude scaling factors at sea level based on the Lifton–Sato–Dunai (LSD)[139] and Lal/Stone scaling models[267] (part **Ba**) and altitude scaling factors for two cut-off rigidities based on the LSD scaling model[139] (part **Bb**). Production of in situ cosmogenic nuclides is dependent upon location on Earth because of shielding effects of atmospheric mass and deflection effects of Earth's geomagnetic field. Production rate will also change through time owing to changes in magnetic field. Production rates of in situ ^{10}Be in quartz as a function of depth (part **Bc**). Production rate by high-energy neutrons is substantially higher at the surface than that by muons but attenuates quickly with depth, meaning that at greater depths muons dominate production of nuclides. Muon production rates from REFS[268,269]. **C** | Global distribution of ^{10}Be and ^{26}Al data from glacial landform (part **Ca**) and modern fluvial sediment (part **Cb**) samples. Despite good global coverage, maps highlight that most studies have focused on mountain terranes of the northern hemisphere with large parts of continents such as Africa and Asia lacking data. Data compiled from ExpAge and OCTOPUS databases. Parts **A**, **Ba** and **Bb** adapted with permission from REF.[270], Mineralogical Society of America. Part **Bc** adapted with permission from REF.[271], Cambridge University Press.

Table 1 | **Cosmogenic nuclides produced in the Earth's atmosphere and their half-lives**

Nuclides	Half-life (years)	Main targets
^{3}H	12.3	O, Mg, Si, Fe (N, O)
^{3}He, ^{4}He	Stable	O, Mg, Si, Fe (N, O)
^{10}Be	1.4×10^{6}	O, Mg, Si, Fe (N, O)
^{14}C	5.7×10^{3}	O, Mg, Si, Fe (N)
^{20}Ne, ^{21}Ne, ^{22}Ne	Stable	Mg, Si, Fe
^{22}Na	2.6	Mg, Si, Fe (Ar)
^{26}Al	7.1×10^{5}	Si, Al, Fe (Ar)
^{32}Si	159	(Ar)
^{36}Cl	3.0×10^{5}	Ca, Fe, K, Cl (Ar)
^{39}Ar	269	Ca, Fe, K (Ar)
^{41}Ca	1.0×10^{5}	Ca, Fe (Kr)
^{53}Mn	3.7×10^{6}	Fe (Kr)
^{59}Ni	7.6×10^{4}	Ni, Fe (Kr)
^{60}Fe	1.5×10^{6}	Ni (Kr)
^{81}Kr	2.3×10^{5}	Rb, Sr, Zr (Kr)
^{129}I	1.6×10^{7}	Te, Ba, La, Ce (Xe)

Cosmogenic nuclides are arranged by mass number. Elements that contribute the majority of production are shown. Parentheses indicate targets of nuclides produced in the Earth's atmosphere.

radioactive noble gas ^{81}Kr with unprecedented sensitivity and considerable impact on geosciences.

Ethics in sampling

The whole rock samples necessary for cosmogenic analysis must be sampled from the landscape, a practice that has recently come under scrutiny as widely used sampling techniques can compromise the aesthetic, historical, cultural or spiritual value of sampled sites[40,41]. Geoethics represents the set of principles at the intersection of geoscience, philosophy, economics and sociology, which can guide geoscientists to collect samples in ways that minimize these deleterious impacts[41]. Yet challenges remain in ethical production of geoscience knowledge. For example, a recent synthesis found that 87% of climate change studies drawn from a global sample spanning 1996–2016 utilized an extractive model "in which researchers use Indigenous knowledge systems with minimal participation or decision-making authority from communities who hold them"[42]. To address this, Indigenous research frameworks can be employed by Indigenous and non-Indigenous researchers to ensure that practices at every step of the research process, including sampling, support transparent communication and, thus, fully adhere to the ethical standards of all communities involved[43]. Other examples of where such frameworks can promote ethical accountability are in publication[43] and data sharing[44]. The CARE principles for Indigenous Data Governance, for example, provide guidance for maintaining Collective Benefit, Authority to Control, Responsibility, and Ethics (CARE) as access to data increases and expectations around data sharing converge towards increasing openness and accessibility[44].

Geochemistry of cosmogenic nuclides

Important areas of geochemical advance include the improved analytical sensitivity and precision of the most frequently used cosmogenic nuclides ^{10}Be, ^{26}Al and ^{36}Cl, including significant lowering of laboratory blanks by high-purity isotope-spike techniques and the reduction of contamination during the geochemical processing of the samples, as well as geochemical processing of samples for the relatively new measurements of in situ ^{14}C and the atmospheric cosmogenic nuclide ^{81}Kr. We present the geochemistry principles for ^{10}Be, ^{26}Al, ^{36}Cl and in situ ^{14}C first, as those isotopes are analysed by accelerator mass spectrometry (AMS), then discuss the geochemistry of ^{3}He and ^{21}Ne that are analysed by noble gas mass spectrometry and, finally, give basic degassing procedures from natural samples for ^{81}Kr that is measured by ATTA.

^{10}Be and ^{26}Al. In 1992, separation and decontamination procedures for large amounts (tens of grams) of quartz were reported[45], providing a geochemical breakthrough for ^{10}Be and ^{26}Al analyses in this mineral (FIG. 2a). This study single-handedly manifested the quartz–^{10}Be–^{26}Al system at the forefront of both surface exposure dating and burial dating. The basic idea of leaching rocks extensively with diluted hydrofluoric acid presented in this milestone paper remains relevant today. Updates have focused on enriching quartz prior to hydrofluoric acid leaching[46], streamlining the column chemistry[47] and drastically lowering the blank levels[47,48]. Improvement of the overall analytical performance of AMS[49,50] has reduced the required sample size and simplified the chemistry.

Quartz remains by far the most widely used mineral for ^{10}Be and ^{26}Al analyses, and is also suitable for ^{14}C and ^{21}Ne measurements. However, other mineral phases have shown promise, in particular for ^{10}Be analyses, including feldspar (such as sanidine)[51] and, most recently, pyroxene[52,53]. As ^{36}Cl and the cosmogenic noble gases ^{3}He (from pyroxene) and ^{21}Ne (from pyroxene and sanidine) can also be analysed from these minerals, new multi-nuclide burial dating application pathways have been opened by this progress.

^{36}Cl. Whereas early ground-breaking ^{36}Cl measurements used whole rock samples[7], the advantages of using clean mineral separates for precise and reproducible ^{36}Cl analysis have become apparent[54]. Feldspar is a common mineral that is suitable for ^{36}Cl applications[54–57]. A technique known as froth flotation is used to separate tens of grams of feldspar from whole rocks and to perform the separation of feldspar and quartz, which has been challenging due to similar physical properties of these two minerals[58,59]. In the first step of froth flotation, chemicals are used to make pre-leached quartz hydrophilic and feldspar hydrophobic. Subsequently, carbonization and addition of oil (pine oil, for example) are used to float the feldspar grains to the foamy top of the solution surface, whereas the hydrophilic quartz sinks. Separation can be executed by simple decantation. Many rocks contain feldspar and quartz, so froth flotation is important to allow for ^{21}Ne/^{10}Be/^{26}Al/^{36}Cl analyses from

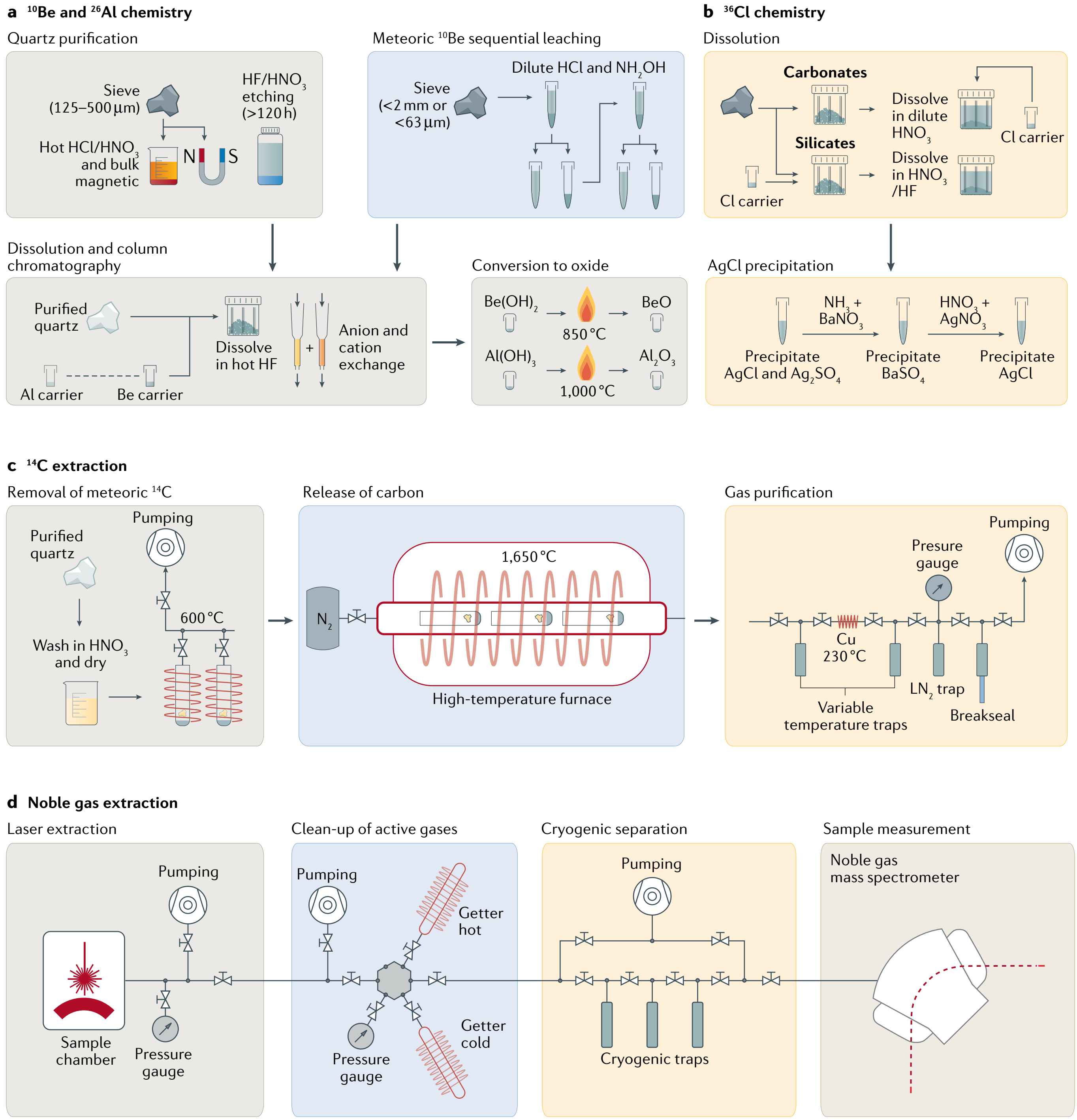

Fig. 2 | **Experimental procedure. a** | Sample preparation protocols for in situ-produced ^{10}Be and ^{26}Al usually involve the following four steps: quartz purification[45]; carrier addition and complete sample dissolution in hydrofluoric acid (HF); isolation of Be and Al using column chromatography; and conversion to Be and Al oxides ready for accelerator mass spectrometry (AMS)[235]. For meteoric ^{10}Be, analyses are performed on bulk sample and mineral separation is not required. Prior to complete HF dissolution, the sample may undergo sequential leaching steps to separate various Be fractions[272]. **b** | ^{36}Cl chemistry depends on the material being analysed (such as silicates versus carbonates) and consists of two major steps: sample cleaning and dissolution; and AgCl precipitation[54]. **c** | Extraction of in situ-produced ^{14}C involves three major steps: in vacuo removal of meteoric ^{14}C; quantitative release of carbon as CO_2 gas; and gas purification and quantitation[65,72]. Exact procedures for each of the above steps depend on design of vacuum extraction system used (for example, REFS[69–72,75,243]). Extracted gas may also undergo a graphitization step if no gas ion source is present[99,101]. **d** | Extraction of noble gases from mineral separates can be done via laser extraction, heating in a furnace or in vacuo crushing. Sample purification is achieved via removal of active gases using variable temperature getters, and use of cryogenic traps to separate various noble gases. Noble gas isotope analyses require complex noble gas mass spectrometers (for example, REF.[108]).

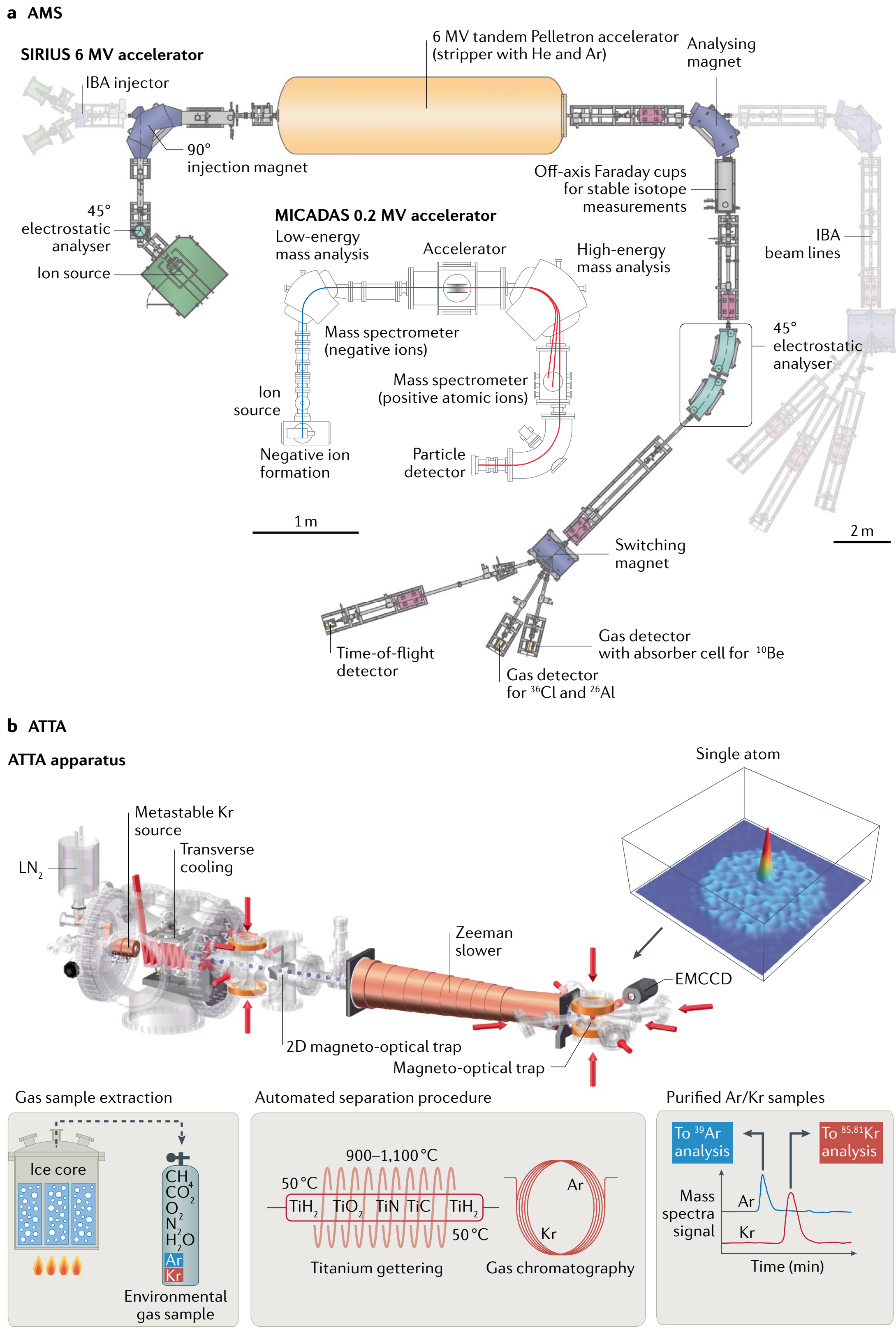

a single sample and facilitating a range of multi-nuclide applications, including burial dating.

More recently, an efficient separation method for larger amounts of clean pyroxene (grams to tens of grams) has been reported[60], which adds another mineral for multi-nuclide applications, as pyroxene is also well suited for ^{3}He and ^{21}Ne (REFS[4,61,62]). Similar advances have been made for ^{36}Cl measurements from magnetite, which have been used to constrain the ^{36}Cl production rate from iron, as well as to derive catchment-average denudation rates from detrital magnetite[63,64]. The challenge remains here to precisely and accurately constrain

Fig. 3 | **Instrumental set-up for AMS and ATTA. a** | Layout of ANSTO's SIRIUS 6 MV accelerator system[50,273] and the 0.2 MV MICADAS accelerator[274]. Despite differences in size and level of complexity, both accelerator mass spectrometry (AMS) systems consist of the following main parts: an ion source that generates negative ions, a low-energy magnetic analyser that separates pre-accelerated ions, an accelerator that breaks up molecules and changes the charge of ions from negative to positive, a high-energy magnetic analyser that separates ions of interest and a detector where measurement occurs. **b** | Atom trap trace analysis (ATTA) apparatus: a neutral atom of a particular isotope (for example, ^{85}Kr, ^{39}Ar, ^{81}Kr) is selectively captured by a magneto-optical trap and detected by observing its fluorescence[275]. ATTA is unique among all trace analysis methods in that its detection is free of interference from any other isotopes, elements or molecules. The high degree of redundancy built into the trapping and detection process, in the form of repeated resonant excitations, guarantees that identification of the targeted isotope is never in error. ATTA sample extraction: a degassing instrument is used to extract gas dissolved in water or trapped in ice, and a purification step is usually required to extract the low levels of Kr and Ar from the bulk gas sample. Sample purification is achieved using cryogenic adsorption, chemical reaction and gas chromatography techniques[83]. EMCCD, electron-multiplying charge-coupled device. Part **a** ANSTO SIRIUS accelerator adapted with permission from REF.[273], Elsevier. Part **a** MICADOS accelerator adapted with permission from REF.[274], Elsevier. Part **b**, image courtesy of University of Science and Technology of China.

the ^{36}Cl production rate, which is overall more complex and, thus, less precisely known than that of ^{10}Be and ^{26}Al from quartz, for example.

In situ ^{14}C. A breakthrough for in situ ^{14}C geochemistry[65] laid the foundation for the application of in situ ^{14}C for timing and quantifying Earth surface processes. Building on early pioneering work[66,67], a reproducible extraction procedure of in situ ^{14}C from quartz is described, which separates the in situ ^{14}C component from organic and atmospheric ^{14}C by stepwise heating of quartz under high-vacuum conditions. The released in situ ^{14}C is completely oxidized to $^{14}CO_2$, as circulating oxygen affords transforming the carbon into $^{14}CO_2$. The CO_2 is then separated from other gases, spiked with a known amount of $^{12}CO_2$, and the ^{14}C/^{12}C or ^{14}C/^{13}C ratio is analysed by AMS. This vacuum extraction procedure was widely adopted and many laboratories still operate modified eponymous Lifton in situ ^{14}C lines (for example, REFS[68–71]). More recently, several laboratories have also developed extraction procedures based on simpler metal-based designs[72–76] (FIG. 2c) that have achieved lower blank levels and shorter extraction times. Although the extraction of in situ ^{14}C from quartz remains challenging and time consuming to date, the scientific appeal and potential of combined in situ ^{14}C, ^{10}Be and ^{26}Al analyses from quartz is substantial enough to motivate further advances in in situ ^{14}C techniques. The short half-life of in situ ^{14}C (5,700 ± 30 years; TABLE 1) is especially suitable for studying the dynamics of glaciers[77–79], fluvial systems[80] and rapid changes in surface processes[81] during the Holocene, the ongoing interglacial period that began 11,500 years ago.

^{3}He and ^{21}Ne. Pyroxene and olivine have been the minerals of choice for both cosmogenic ^{3}He and ^{21}Ne analyses, followed by quartz, which does not quantitatively retain ^{3}He but retains ^{21}Ne. Traditionally, physical mineral separation methods have been used to separate the smaller amounts (tens of milligrams to 1 g of mineral) needed for the noble gas isotope analyses. However, the acid leaching method[45] discussed above for ^{10}Be and ^{26}Al geochemistry (FIG. 2a) can be used to measure ^{21}Ne from quartz as well, and is thus useful for multi-nuclide measurements from quartz. Recently, a similar hydrofluoric acid leaching method was presented for separating larger amounts (several grams or more) of fine-grained pyroxene[60]. This progress to separate large and clean amounts of pyroxene opens the prospect of using ^{36}Cl/^{3}He dating methods from this mineral, as ^{36}Cl is produced from calcium (and pyroxenes typically contain calcium levels up to 10%).

^{81}Kr. ^{81}Kr is a cosmogenic radionuclide that is produced in the atmosphere. Spallation reactions and neutron activation of stable krypton in the upper atmosphere[31] produce ^{81}Kr (half-life of 230,000 years). Because ^{81}Kr has a long residence time in the atmosphere, it is uniformly distributed throughout the atmosphere with an isotopic abundance of 9×10^{-13} (REF.[82]). The ^{81}Kr that is dissolved into water or trapped in ice, which is only about 2% of the total ^{81}Kr inventory, represents a chemically inert tracer of these samples with a simple transport mechanism in the environment. The ^{81}Kr decay decreases the ^{81}Kr/Kr ratio of 9×10^{-13} with time, which is used in dating of old ice and groundwater.

A system for degassing trapped air from ice samples[34] is illustrated in FIG. 3b. The ice is placed in an airtight tank. The atmospheric air in the system is first pumped out. The tank is then heated to melt the ice and release the trapped air, which flows through a water filter and is compressed into a sample cylinder. Krypton and argon are separated from the released sample gas by titanium gettering and gas chromatography techniques[83]. Within 90–120 min of processing time, about 0.5–4 L standard temperature and pressure (STP) air samples can be purified, with purities and recoveries of >90% for krypton (and >99% for argon).

AMS analyses of cosmogenic nuclides

AMS uses an analytical instrument, combining particle accelerator techniques into a mass spectrometer[84] (FIG. 3a). AMS was originally designed for the measurement of ^{14}C/C ratios[85–87], and has been extended to other isotope ratio measurements of interest for geosciences, including the cosmogenic radioisotopes discussed here (TABLE 1). AMS is designed to separate out interferences and count single atoms of one very rare isotope (such as the cosmogenic nuclides ^{10}Be, ^{26}Al, ^{36}Cl and ^{14}C) in the presence of the stable isotopes with up to 10^{15} or even 10^{16} times higher abundances. This outstanding sensitivity transformed cosmogenic nuclide methods, and has been a key driver of progress over the past 40 years.

Consistent with the last section, we briefly review recent progress and the current sensitivity and analytical limits of cosmogenic nuclide in AMS analyses based on the analyte.

^{10}Be. Since the original breakthrough in the 1970s (REFS[88,89]), the sensitivity of ^{10}Be measurements with AMS has further improved, making ^{10}Be a widely applied cosmogenic nuclide in geosciences. Dramatically improved counting statistics[90–93] together with low ^{10}Be procedural blanks of <10,000 ^{10}Be atoms now allow sample measurements of as few as 10,000 ^{10}Be atoms, widening the application spectrum and improving uncertainties. For example, ^{10}Be techniques now allow for surface exposure dating of surfaces as young as a few decades, which overlap with historic records, reports and even photography[94].

^{26}Al. Similar AMS advances have been made for low-level/high-sensitivity ^{26}Al measurements. Successful implementation of a gas-filled magnet[95] to the AMS line has improved the counting statistic by an order of magnitude[96], and now the precision of $^{26}Al/^{27}Al$ measurements can approach that of $^{10}Be/^{9}Be$ measurements[93]. However, the notorious problem of laboratory-specific measurements of the stable and abundant ^{27}Al in geological samples (such as quartz separates from surface rocks) remains a source of substantial uncertainties, motivating systematic and community-wide cross-calibration programmes for the comparably simple ^{27}Al concentration measurements.

^{36}Cl. ^{36}Cl analytics, and thus applications, have considerably progressed with the pioneering study measuring ^{36}Cl in seawater[97], where the authors present measurements and the underlying spiking and low blank techniques of $^{36}Cl/Cl$ ratios as low as 5×10^{-16} and blank levels as low as a few thousand ^{36}Cl atoms. The presented geochemical and analytical techniques afford low-level ^{36}Cl measurements in rocks and sediments, which is particularly relevant for burial dating techniques — for example, for surfaces underneath ice sheets that have been previously exposed during prior warm periods for a few thousand years and, subsequently, buried by the ice sheet for tens or, even, hundreds of thousands of years. The high-sensitivity cosmogenic nuclide methods described here are central to these ice sheet stability applications using sub-ice bedrock.

In situ ^{14}C. Although several AMS facilities are able to perform measurements of $^{14}C/^{13}C$ and $^{13}C/^{12}C$ of single conventional radiocarbon targets with precisions as low as 0.2%[49,98], measurements are more problematic when samples contain a few micrograms of carbon — such as the case of samples analysed for in situ ^{14}C. The measurement of these samples has been aided by the development of laser-heated graphitization microfurnaces allowing the complete graphitization of samples containing as little as 2 µg of carbon[99], as well as the development of more versatile gas ion sources[100,101]. The latter is especially important for in situ-produced ^{14}C as the minute amount of carbon extracted as CO_2 from quartz samples does not need to be spiked and can be analysed directly. The elimination of the need to graphitize reduces sample processing times and AMS measurement times, and supresses contamination introduced during graphitization. Samples can now be delivered as pure CO_2 in glass ampoules and yield reproducibly good $^{12}C^-$ currents with better counting statistics[101].

^{53}Mn. A few recent studies reported measurements of ^{53}Mn from terrestrial rocks[102], and present a first-order production rate of ^{53}Mn from iron[103]. The advantage of ^{53}Mn is its long half-life of 3.7 Myr, which in theory allows for $^{3}He/^{53}Mn$ burial dating on timescales of many million years. This would be very valuable to tackling long-term Antarctic ice sheet fluctuation problems, for example. However, ^{53}Mn remains difficult to analyse, so the application remains very rare.

Noble gas mass spectrometry

Noble gas mass spectrometry measures isotopic ratios of small quantities of noble gases and, similar to AMS, affords measurements of rare isotopes, such as ^{3}He, in the presence of 10^{16} times more of the other helium isotope, ^{4}He. Noble gases are released from the samples either by laser or furnace techniques, under ultra-high-vacuum conditions (pressure $<10^{-9}$ mbar) into an extraction line directly connected to a mass spectrometer. Noble gas isotope ratio measurements are performed by static-mode analysis, whereby gas is trapped in the mass spectrometer volume for the entirety of the measurement. Pioneering work was published as early as the 1940s[104], high-sensitivity measurements reported in the 1950s[105] and cosmogenic helium[4,39] and cosmogenic neon[3,106,107] studies were published decades later.

A new generation of multi-collector mass spectrometers — such as the HELIX MC Plus multi-collector noble gas mass spectrometer — presents a significant step forward[108], and opens new pathways for cosmogenic ^{21}Ne applications, in particular in combination with ^{10}Be and ^{26}Al analyses from the same quartz samples[20].

In addition, cosmogenic ^{38}Ar measurements from terrestrial rocks[109] were reported, followed by a first-order ^{38}Ar production rate determination from pyroxene[110]. Owing to the very high atmospheric argon background, cosmogenic ^{38}Ar applications might be limited to long-exposed surface rocks with high cosmogenic inventory, but the ^{38}Ar production from calcium and potassium has the potential to open ^{38}Ar surface exposure dating of feldspar.

ATTA measurement

Analytical instruments based on the ATTA method are operational in the United States, China, Germany and Australia[33]. In ATTA, a magneto-optical trap[111] is used to selectively capture and detect neutral atoms of the targeted isotope (FIG. 3b). When the laser frequency is tuned to the resonance of this isotope, for example ^{81}Kr, the atom is repeatedly excited at the rate of $10^{7}\,s^{-1}$. As a result, the atom can be confined by the photon scattering force and detected by observing its fluorescence. This process of repeated resonant excitations guarantees that the identification of the targeted isotope is free of interference from any other isotopes, elements or molecules.

Results

Surface exposure dating

The concentration of cosmogenic nuclides in a specific surface sample divided by the cosmogenic nuclide production rate yields the duration that the surface has been exposed to the open sky, and thus to cosmogenic nuclide bombardment. This is referred to as the surface exposure age (FIG. 1). Various geomorphic assumptions need to be realized to make the surface exposure age reliable, such as continuous, uninterrupted and unshielded exposure of the sample surface to cosmic rays[9,11,112], and the assumption of no erosion or known erosion of the sample during exposure. The strategy of dating many samples from one geomorphic unit has proven effective in improving the robustness of surface exposure dating despite complex geomorphic processes[48,62,113–126]. But even if all geomorphic parameters are controlled, surface exposure dating can only be as accurate and precise as its two basic parameters: the measured concentration of cosmogenic nuclides in a sample and the production rate of cosmogenic nuclides in this surface, which varies with altitude, latitude and time of exposure, and is to some degree nuclide-specific.

The improvement in cosmogenic nuclide geochemistry and analytics discussed above have moved the needle, and better measurements (and models) yield surface exposure ages with smaller uncertainties. It is not our goal here to put to rest the decade-long discussion about precision and accuracy of surface exposure dating — we attempt to provide a snapshot together with a projection forward.

Production rates and production models. The rate of cosmogenic nuclide production at selected points can be experimentally determined, and particle physics-based production models are used to interpolate between those point measurements, so any location on earth has an assigned cosmogenic nuclide production rate within its uncertainties. The idea of a cosmogenic production rate calibration experiment is simple: a surface with unambiguous and simple geomorphic context whose formation/onset of exposure has been independently and robustly dated is sampled and the cosmogenic nuclide inventory is analysed as precisely as possible. Dividing the measured cosmogenic nuclide concentration by the independent duration of exposure yields the cosmogenic nuclide production rate. This rate is typically given in produced atoms per gram of mineral and per year. Examples include deep-seeded landslides that, for example, killed and buried trees or macro-organics that can be precisely radiocarbon dated[127,128]. Well-mapped and radiocarbon-dated moraines are another good target for successful production rate experiments[129–131].

Uncertainties of local production rate experiments, as well as those of production models, have been a topic of intense efforts and discussion. Although the precision of the cosmogenic nuclide measurements has improved, the handling of earlier and recent production rate calibration experiments as well as production rate scaling models have remained controversial topics[38,132].

By far the most comprehensive collection of cosmogenic nuclide production rate experiments, and in fact the first consistent and organized cosmogenic database, is presented by the ICE-D production rate calibration data compilation[16]. ICE-D reports ^{10}Be, ^{26}Al, ^{3}He and ^{21}Ne production rate experiments comprehensively, and has recently started to include ^{36}Cl production rate experiments.

The few calibration experiments for the in situ ^{14}C production rate are not yet included in the ICE-D, but there have been reports of consistent values of 11.4 ± 0.9 atoms g^{-1} year^{-1}, 12.0 ± 0.9 atoms g^{-1} year^{-1} and 11.2 ± 0.6 atoms g^{-1} year^{-1}, scaled by convention to sea level/high latitude[133–135]. There is clear need for more such experiments from a wide variety of in situ ^{14}C laboratories.

The ICE-D database highlights the trajectory of production rate determinations, from pioneering early experiments to more recent higher precision ones. Overall, the best constrained production rate calibration experiments show an encouraging trend to higher precision and accuracy of the individual experiments and a converging trend of the production rate values, with variations between these recent production rate calibrations in the 5% range[17]. Given how different the geomorphic settings and climate zones of these experiments are (from the polar regions to the tropics, and from sea level to altitudes above 4,000 m), the level of consistency and the observation of a converging trend are encouraging and the cosmogenic nuclide geosciences community is likely to see a further refinement of the production rate values and, thus, the surface exposure dating method in the coming years.

Cosmogenic nuclide production models simulate the transport of the secondary cosmic ray neutrons and muons through the atmosphere to the Earth's surface and the different cosmogenic nuclide production reactions, based on nuclear and particle physics theory (FIG. 1A,B). These models provide theoretical cosmogenic nuclide production rates through the atmosphere to the earth surface, and describe the spatial and time-dependency of cosmogenic nuclide production reactions as functions of altitude, latitude and time. Pioneered by Lal et al.[5,136], several powerful models have been presented over the past decade[137–140]. Such models are essential to interpolate between the production rate calibration points that are singular in space and time, and are implemented in the rapidly improving cosmogenic nuclide calculator modules that are widely used by the community and allow, for example, calculation of exposure ages and erosion rates from cosmogenic nuclide measurements within an internally consistent and well-documented framework (for example, REFS[141,142]).

Another recent advance based on these models is the realization that the production rates for different cosmogenic nuclides, in other words the production ratio of two different cosmogenic nuclides, vary considerably with depth — both in the atmosphere and in the rock — a critical observation for burial dating[137,138].

Surface exposure dating range. The oldest surface exposure ages reported to date rely on the stable cosmogenic noble gases ^{3}He and ^{21}Ne, and now reach back into the Miocene (FIG. 4). For example, a recent study presents a stunningly consistent cosmogenic chronology constraining East Antarctic Ice Sheet fluctuations over the past 14.5 million years[62]. On the young end, over the past decade surface exposure dating with ^{10}Be — and also ^{3}He — has been used to date surfaces exposed over the past millennium[143]. One prominent example is the late Holocene moraine chronologies that constrain glacier advances during the Little Ice Age period (~1300–1850 CE) with centennial resolution[48,79,144–148]. This recent advance

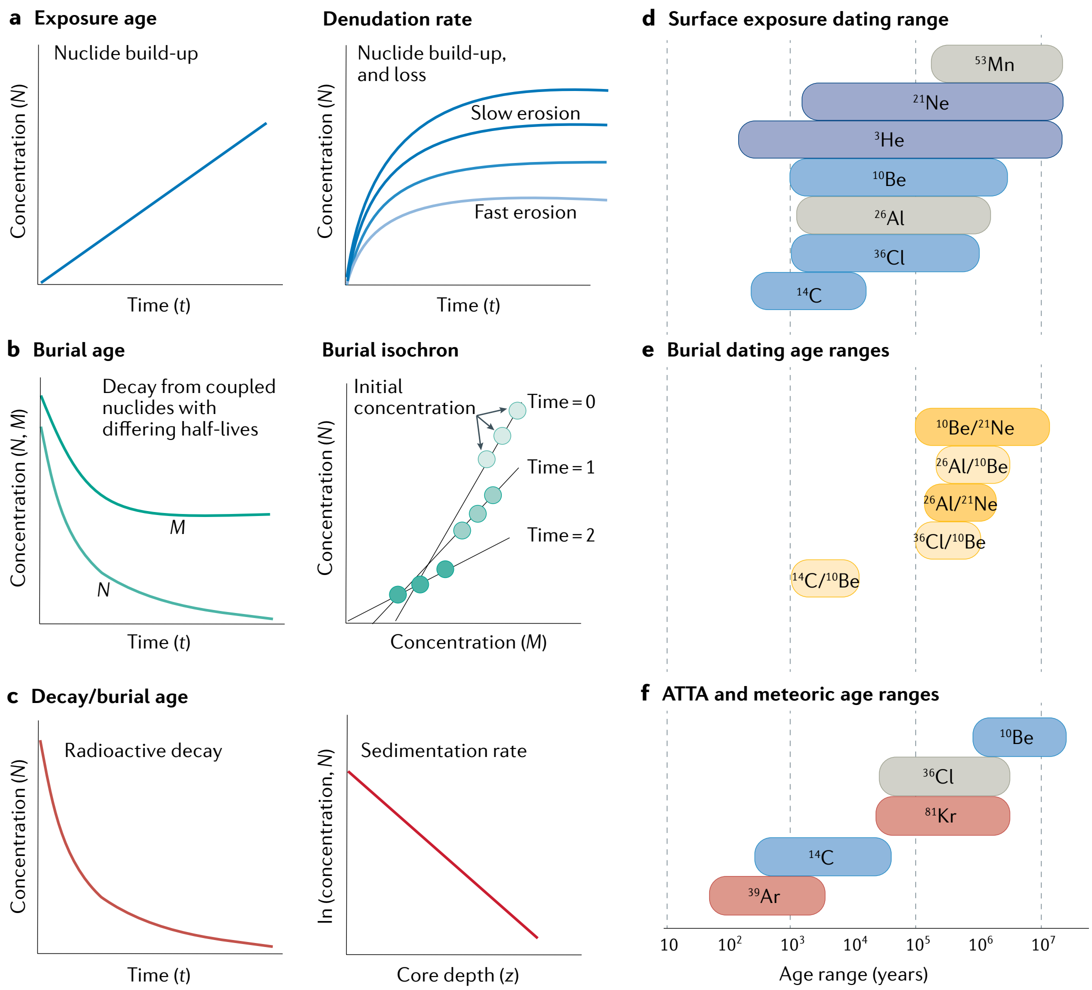

Fig. 4 | **Representative results. a** | Over time, concentration of cosmogenic nuclides increases with continued exposure to cosmic radiation (left). Denudation causes a sample's cosmogenic nuclide inventory to decrease (right). Rate of erosion sets the maximum concentration a surface can attain. **b** | If a sample is exposed to cosmic radiation, then buried and shielded from further production of cosmogenic nuclides, radioactive elements will decay according to their specific half-lives. Two (or more, not pictured) nuclides with differing half-lives can be used together to date burial age (left). Burial techniques have benefitted from plotting isochrons (right). In this case, starting ratio of two nuclides is set at the surface and changes during even shallow burial. Noting that if starting concentrations for individual samples are often different, slopes of lines that plot through the data can be used to calculate age of the deposit. **c** | For nuclides that originate in the atmosphere, starting concentrations decay with characteristic half-lives. Such techniques have been used to measure sedimentation rates and with the advent of atom trap trace analysis (ATTA), old ice and groundwater can also be dated. **d** | Age range of surface exposure dating, that depends on the radioactive half-life/stability of the nuclide. **e** | Age range of burial dating depends on radioactive half-life of nuclide pairs. Values of ratios are set via production and diverge from those values after burial. **f** | In ATTA (^{81}Kr and ^{39}Ar) and for meteoric nuclides (^{14}C and ^{10}Be), initial nuclide concentration is set in the atmosphere and when the gas is sealed from contamination with modern air, nuclides decay over time. Parts **a**, **b** and **c** adapted with permission from REF.[276], Mineralogical Society of America.

allows for a comparison of cosmogenic chronologies with historic and photographic records[94,149].

Burial dating

The most widely used cosmogenic nuclide burial dating tool is ^{26}Al/^{10}Be with a production ratio during exposure in the mineral quartz constrained to about 6.75–7 (REFS[20,150]). During burial, the ^{26}Al/^{10}Be ratio changes with an 'apparent half-life' of about 1.5 Myr. This means that a previously exposed quartz mineral containing seven times more cosmogenic ^{26}Al than ^{10}Be, which gets buried deep enough that the cosmic ray production ceases for 1.5 Myr, shows a ^{26}Al/^{10}Be ratio of 3.5 after this burial period.

The ^{26}Al/^{10}Be burial dating range is from about ~300 kyr to several millions of years (FIG. 4). Other cosmogenic nuclide systems, such as ^{36}Cl/^{10}Be, have been successfully applied and are poised to become increasingly important[151] (FIG. 4). Triple isotope burial dating studies using, for example, ^{10}Be, ^{26}Al and ^{21}Ne from quartz[20] as well as recent burial dating isochron techniques[20,112,152] have been shown to further push the limits of burial dating, providing answers to new questions about Earth's surface.

Denudation rates

Measuring denudation rates derived from meteoric, and later, in situ-produced cosmogenic nuclide concentrations has revolutionized quantitative geomorphology over the past several decades. But now, the field has gone beyond simple documentation of rates for different settings[153,154] and timescales[155], and has moved to testing assumptions regarding the controls on denudation and landscape evolution. Some of the results give us no surprises in hindsight, such as the increase of denudation rates in the proximity of fault scarps[156] and the inverse relationship between soil depth and the production of soil[157], but some truly challenge our preconceived assumptions such as the lack of correlation of basin-wide denudation rates with modern precipitation rates[25] and the negligible effect of glaciation on global denudation rates[26].

The averaging timescale undergone by particles moving through the production zone[25] and the geomorphic system can affect their sensitivity to measuring erosion rate change due to perturbations such as climate or land use[158]. Several parts of the geomorphic system can buffer environmental signals[159]. Thick soils buffer changes in erosion more effectively than thin soils (FIG. 5). Floodplains can either cause cosmogenic nuclide signals to be faithfully transmitted[28], gain cosmogenic nuclides during transport[80] or lose cosmogenic nuclides through decay during transport[29] (FIG. 5). Long integration times can make it impossible to observe the potential impact of climate on denudation through time. In this case, when we do not see changes in erosion over long periods of time, it is unclear what is causing that stability, whether it is actually unchanging erosion rates or a well-buffered system that does not easily respond to perturbations[160–163].

ATTA of ^{81}Kr

An atom trap is used to capture and count ^{81}Kr atoms from a purified krypton sample, generating an atom count rate that is proportional to the isotopic abundance of ^{81}Kr. The resulting isotopic abundance of the sample, compared with that of the atmosphere, is used to calculate the ^{81}Kr age based on a simple nuclear decay formula. Recent studies illustrate how ATTA results can be used to answer key questions in geoscience. In hydrology, ^{81}Kr studies of large aquifer systems around the world have transformed the understanding of their long-term behaviour, revealing recharge histories and leading to improved hydrodynamic models[164–169]. Cross-comparisons between measurements of ^{81}Kr and other tracers (^{4}He and ^{36}Cl) have also been made[170–172]. In glaciology, ^{81}Kr dating of old Antarctic ice, first demonstrated with the well-dated stratigraphy of Taylor Glacier[173], has been used to establish a new TALDICE-deep1 chronology[174].

^{81}Kr dating has since been applied to search for old ice in the Tibetan Plateau[34] and to provide anchor points for a new age scale for the deep portion of TALDICE ice core in East Antarctica[175].

Applications

We focus here on two complementary applications at the forefront of cosmogenic nuclide geosciences, with the goal of illustrating the power of cutting-edge cosmogenic nuclide dating methods in addressing key questions of geomorphology, Quaternary geology, climate and society, now and in the coming decades.

Erosion factories over space and time

One way to unravel the influence of different driving forces of landscape change — including tectonic uplift and climate, as well as internal dynamics such as river drainage capture and subsidence, among others — is to develop quantitative constraints on the magnitude, rate and timescale of surface change. Quantifying how these processes shape landforms is crucial for modelling past and future landscapes. Even Earth system-scale carbon cycle models rely on understanding the dynamic linkages between climate and tectonics stemming from the empirical relationship observed between rates of chemical weathering of minerals and physical erosion[176], which scales with topographic relief (FIG. 5). This dynamic interaction of climate and tectonics can alter the chemistry of the atmosphere and ocean via Earth's carbon cycle and alkalinity budget.

In mountainous environments, measured denudation rate values span almost four orders of magnitude from <1 mm kyr^{-1} to >10^{3} mm kyr^{-1} (REF.[154]). This range is similar to that measured by other techniques[177]; however, cosmogenic nuclide rates average over timescales better mirroring those of geomorphic processes and the rates imposed by them. An apparent erosion rate or exhumation of soil grains from ^{10}Be and the relatively new in situ ^{14}C clock depends not only on the erosion rate but also on the half-life of the radionuclide. Because of its short half-life, in situ ^{14}C records recent variations in erosion, including timing and magnitude of the change in erosion[178,179]. The concentration of the cosmogenic nuclide with the shorter half-life adjusts faster to a changing erosion signal, and thus changing erosion creates a systematic and measurable offset between in situ ^{14}C (or ^{26}Al) and ^{10}Be (REF.[178]).

Control of denudation rates. Rivers sample minerals from source locations in the fluvial network (that is, bedrock substrates and hillslopes) according to the erosion rate of that particular subregion in the landscape. The minerals contain measurable cosmogenic nuclide concentrations that are quantitatively governed by the denudation rate. Bedrock knobs protruding above the soil-mantled slopes, for example, have higher concentrations of cosmogenic nuclide precisely because they are not eroded as much as the sediment in the catchment's hillslopes, and therefore are not sampled as often (FIG. 5).

Basin-wide denudation rate compilations have been used in the past decade to understand global controls on denudation that can be counter-intuitive, with the most obvious triggers of sediment transport and chemical weathering not tied in an obvious way to the denudation rate[180–182]. For example, some of the hottest[183] and rainiest[184] places on Earth erode relatively slowly — as do hot and rainy places[185,186] — whereas the basin slope has consistently emerged as a primary control in tectonically active areas (FIG. 5).

Variations in palaeo-denudation rates, on the other hand, have been ascribed to changes in precipitation[187–190] or temperature[191,192], or climate generally[193–195]. Other causes of variations in denudation rates can be linked to the subsidence of the basins[196,197]. Measured palaeo-denudation rates in the Tianshan of Central Asia — a region particularly important because of a famous argument for the impact of climate on denudation rates — show the absence of a major increase in denudation rates with the onset of continental glaciations 2.6 million years ago in the region[198,199]. Over glacial–interglacial cycles, rates can also show a pulsed,

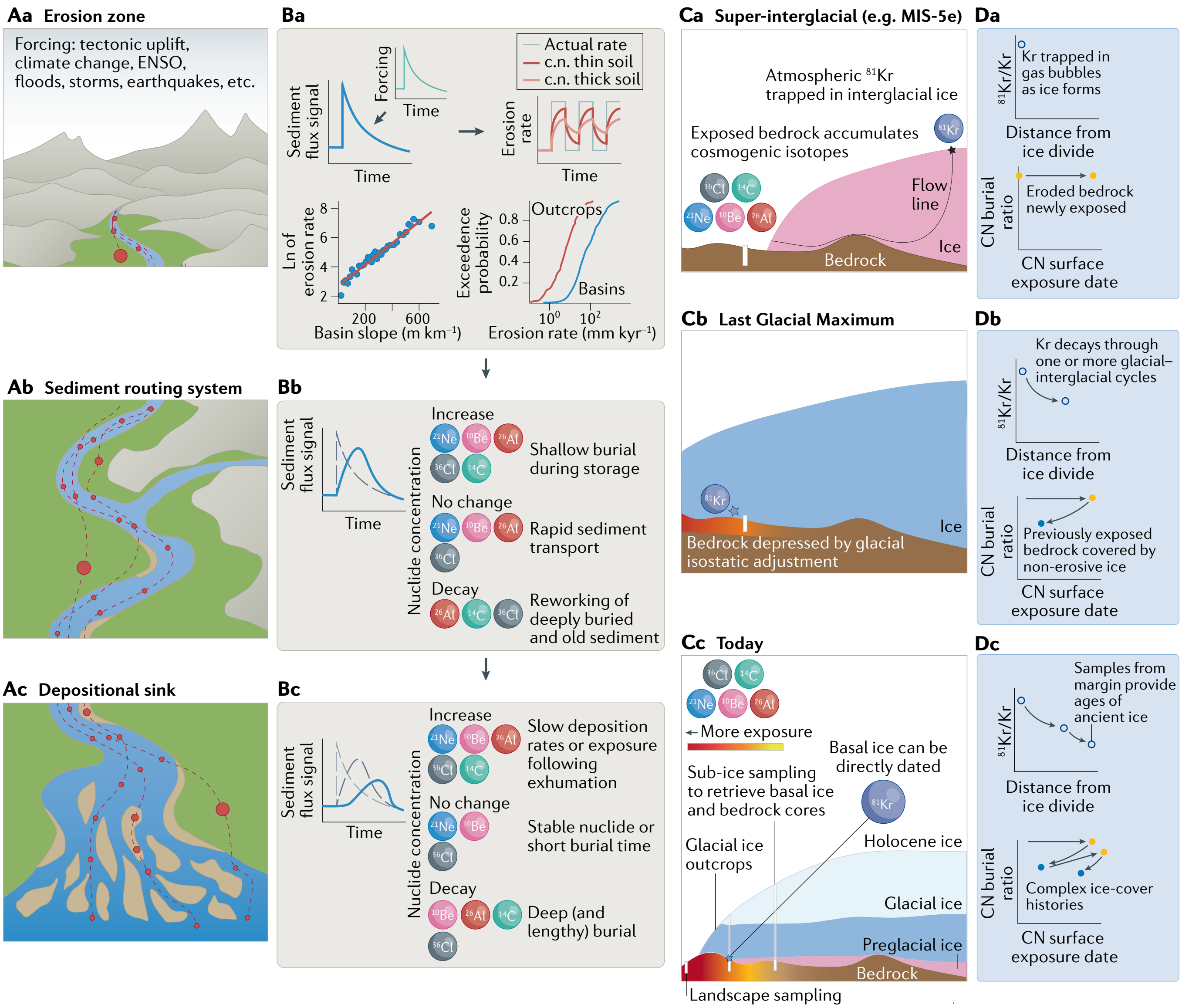

Fig. 5 | **Applications of cosmogenic nuclides to studying source-to-sink processes and the history of the Greenland Ice Sheet. A,B** | Erosion in mountains is affected by various tectonic, climatic and autogenic factors. Sediment pulse makes its way out of the erosion zone (part **Aa**), through the sediment routing system (part **Ab**) and into the depocentre sink (part **Ac**) along trajectories shown by red dashed lines. Some trajectories involve short transit times with brief periods of storage (small circles) whereas others involve longer transit times with protracted periods of storage (large circles)[159]. Signal of the slug of sediment from episodic forcing in the source and the resulting observed erosion rates signal is buffered and changes over time as it moves through the routing and sedimentary system (parts **Ba** to **Bc**). At source, changes in erosion rate will result in changes in nuclide concentration, moderated by response time of the cosmogenic nuclide clock[277]. Using compilations of global cosmogenic nuclide-based rates from erosional systems, basin-wide denudation rates scale exponentially with mean basin slope[154,181] and protruding outcrops of bedrock erode slower than do the basins suggesting widespread relief generation[180]. Following detachment from bedrock, the cosmogenic nuclide inventory in a parcel of sediment may increase, decrease or stay constant, depending on characteristics of the sediment routing system (part **Bb**), rate of deposition in the sink (part **Bc**) and nuclide half-life. **C** | Three snapshots of Greenland Ice Sheet depicting retreat during a hypothetical super-interglacial[278,279] (part **Ca**), advance during the Last Glacial Maximum[280] (part **Cb**) and today (part **Cc**). Colours within ice sheet indicate ice of different ages: super-interglacial (pink), glacial (dark blue) and postglacial or Holocene (light blue). Black line in part **Ca** shows trajectory of ice with trapped atmospheric ^{81}Kr. In parts **Cb**,**Cc**, same ice parcel indicated with purple star. White rectangles show where rock cores collected from the landscape can be analysed with cosmogenic nuclides to constrain the footprint of the ice sheet in the past (for example, REF.[213]). **D** | Schematic volution of ^{81}Kr/Kr ratio for ice parcel shown by purple star, and cosmogenic nuclide concentration and burial ratio for the rock core recovered from beneath the ice (parts **Da**–**Dc**). c.n. and CN, cosmogenic nuclide; ENSO, El Niño-Southern Oscillation. Part **A** adapted from REF.[159], Springer Nature Limited.

ephemeral response to climate, with a short-lived spike in erosion during maximum glacial expansion[200]. More studies in the coming years will likely add to denudation and palaeo-denudation rate data and the nuanced interpretations of controls over time, although we can already say that the erosion engine is primarily fuelled by tectonic energy creating a conveyor of crustal material that can sustain denudation at high rates for long periods of time.

Ice sheet stability

Rising sea levels threaten coastal communities and ecosystems, and by mid-century, melting polar ice sheets will be the dominant driver of sea level rise (IPCC SR15 report[201]). The melting Greenland Ice Sheet holds 7 m of sea level equivalent, and is becoming the focus of particular scientific concern[202,203] with new estimates predicting that the Greenland Ice Sheet melt rate this century will exceed any melt over the past 10,000 years (REF.[204]).

Cosmogenic nuclide geosciences have contributed to a much improved understanding of margin changes of the Greenland Ice Sheet over the ongoing warm period, the Holocene (the past 11,700 years)[79,117,120,124,126,205–208]. Marine and ice core records have been interpreted as indications for a relatively persistent, stable Greenland Ice Sheet[209–211]. Relatedly, folded ice in the lowest part of the North Greenland Eemian Ice Drilling (NEEM) ice core is reported to be from the last interglacial period (Eemian or MIS-5) and the isotope signals indicate relatively moderate response of the Greenland Ice Sheet to the MIS-5 super-interglacial that was likely significantly warmer than today[212].

Two recent cosmogenic nuclide-based pilot studies, however, present the first direct evidence about past periods of a greatly reduced Greenland Ice Sheet in the recent geologic past: a ^{10}Be/^{26}Al depth profile from the 1.5 m-long GISP2 bedrock core, retrieved in 1996 under the more than 3,000 m-long GISP2 ice core, showed that Greenland was nearly ice-free at least once, and probably several times, over the past 1.1 Myr[213]. The cosmogenic nuclide pilot data from frozen sediment under the Camp Century ice core, drilled to 1,368 m in 1966, detail a similar result for the Camp Century sediments[214]. These two studies not only highlight the vulnerability of the Greenland Ice Sheet to warming but also show that the basal zone preserves information about past exposure and subsequent reburial by the Greenland Ice Sheet. In other words, these two-point studies from sub-ice material show that cosmogenic nuclide techniques can be used to cosmogenically map the bedrock under the Greenland Ice Sheet, and thus the response of various sectors of the Greenland Ice Sheet to past warm periods.

Motivated by these cosmogenic nuclide findings, we here focus on a novel approach applying cosmogenic nuclide techniques to the Greenland Ice Sheet basal zone to tackle the Greenland Ice Sheet (in)stability problem. Combining cosmogenic nuclide analyses from sub-Greenland Ice Sheet bedrock (and sediment), mapping the bedrock for past exposure and reburial with a systematic cosmogenic ^{81}Kr dating effort of the basal ice, the oldest ice in Greenland, is now possible; the first steps in this direction have been taken[215]. New modelling concepts are presented as tools to synergize the cosmogenic nuclide data from the Greenland Ice Sheet basal zone, towards an improved understanding of Greenland Ice Sheet deglaciation and re-glaciation processes.

Basal zone
The lowermost tens of metres of ice, the upper metres of sub-ice bedrock and the potential sediment layer in between.

FIGURE 5C,D illustrates the general approach and potential of such a cosmogenic nuclide basal zone study for the Greenland Ice Sheet as an example, but it is important to note that similar approaches can be, and are now being, pursued for other ice sheets, including the Antarctic ice sheets. Key questions about the duration of exposure of bedrock — currently resting underneath hundreds or thousands of metres of ice — during past warm periods, which relates to the length of time the Greenland Ice Sheet was diminished and retreated inland, can now be addressed by this approach.

A strategic drilling transect through the Greenland Ice Sheet into crystalline bedrock and analysing ^{10}Be, ^{26}Al and ^{21}Ne from quartz and ^{36}Cl from feldspar is at the core of such an ice sheet stability experiment. As a first step, such a survey along the Greenland Ice Sheet would identify bedrock segments that were most recently exposed in response to warming, and thus most vulnerable to ongoing climate change. These sections are likely the most vulnerable in the future. Ice sheet modelling techniques depicted in FIG. 5 also allow for estimates of sea level contributions of the cosmogenically reconstructed footprints of the Greenland Ice Sheet.

To determine the age of the basal ice in Greenland, as well as the age and location of the oldest ice, basal ice dating by ^{81}Kr ATTA measurements of strategically drilled basal ice might open new opportunities. The much improved analytical sensitivity of ^{81}Kr ATTA measurements, its uniquely appropriate dating range (FIG. 5) and the robustness of the ATTA analyses against impurities in the ice make this technique ideally suited to tackle the challenge to date old ice in the basal zone of ice sheets. The current limitation remains the need for relatively large ice samples (2–4 kg ice per sample), but as the ATTA method continues to advance, the sample size requirement can be brought to its fundamental limit below 1 kg, with the precision limited by ^{81}Kr atom counting statistics.

Cutting-edge cosmogenic nuclide analyses from sub-ice sheet bedrock together with cosmogenic ^{81}Kr dating of basal ice, synthesized within an ice sheet modelling framework, are poised to directly map the response of the Greenland Ice Sheet to past warm periods. Such insights would transform our understanding of the Greenland Ice Sheet sensitivity to changing climate and enhance our capability to monitor, understand and robustly predict its contribution to sea level rise in the near future, including the contribution over the next decades. In turn, this novel application of advanced cosmogenic nuclide techniques to the basal zone of ice sheets is going to contribute in significant ways to tackle some of the most urgent problems at the interface of geoscience and society.

Additional cosmogenic nuclide results

We close this section with a subjective list of additional applications that are particularly promising and/or trail-blazing. In the field of active tectonics, one application used single grain measurements on alluvial fan surfaces that together form age populations with characteristic distributions to reveal whether sediment is from episodic (landslide/earthquake) or diffusive (soil transport)[216] processes and bear on the interpretations of fault-activation chronologies. Others have pioneered a new method to date precariously balanced rocks in tectonically active regions that would have toppled during vigorous ground shaking in order to reconstruct strong-earthquake recurrence histories[217,218]. In the area of coastal hazards, landslide dating[219] and a new method to measure rates of coastal cliff retreat from cosmogenic nuclide concentrations in bedrock shore platforms[220] can now be transported to other areas to provide a long-term baseline rate for eroding coastlines under threat from current and future sea level rise. Large, mega-tsunami-transported boulders deposited hundreds of metres above the Santiago Island coastline in the Cape Verde archipelago were dated by cosmogenic nuclide analysis to roughly 73,000 years ago, constraining the timing of the collapse of Fogo, an oceanic volcano[221]. One particularly clever cosmogenic nuclide application brings about a new field of cosmogenic nuclide palaeothermometry[222,223]. These authors pioneer the use of temperature-dependent diffusion behaviour of some noble gases, such as cosmogenic ^{3}He diffusion in quartz, to help us answer questions related to long-term climate change and extraterrestrial conditions[224]. Finally, the application of cosmogenic nuclide burial dating to fossil-bearing cave deposits has made important contributions to our understanding of early human evolution[225]. Isochron burial dates from cave infills at Sterkfontein, South Africa, make a convincing case that the skeletons at Sterkfontein are coeval with early *Australopithecus afarensis* in eastern Africa, raising new questions about early hominid diversity and phylogenetic relationships[96].

Reproducibility and data deposition

Precision and accuracy

It is now possible to measure cosmogenic nuclide abundances at total measurement uncertainties of a few per cent. Recent global compilations of in situ cosmogenic ^{10}Be and ^{26}Al confirm the steady improvement in measurement quality (FIG. 6), but at the same time paint a more complex picture. For example, whereas ^{10}Be measurement uncertainties have, on average, improved steadily over the past three decades, substantial scatter is still observed in ^{10}Be uncertainties reported in the past 5 years. The latter reflects, beyond the inter-laboratory uncertainties, the systematic uncertainties related to sampling in complex geologic and geomorphologic settings in the field, an uncertainty within cosmogenic nuclide applications that remains difficult to quantify.

Measurement precision is, however, only part of the story and the improvement in analytical precision does not directly translate into improved accuracy. The CRONUS-Earth and CRONUS-EU projects[38,226], concluded more than 5 years ago, produced a comprehensive suite of reference materials that, in turn, supported several laboratory inter-comparison exercises aimed at improving our understanding of the true precision and accuracy of nuclide analyses (FIG. 6). Results to date from these laboratory inter-comparison exercises show that whereas the analytical uncertainty of ^{10}Be measurements explains most of the variation in the data sets[227,228], coefficients of variation exceed the average analytical uncertainty for most materials and nuclides (see REF.[38]). The latter effect is strongest for the rather novel in situ ^{14}C and the still complex ^{21}Ne measurements, for which substantial inter-laboratory and intra-laboratory variability is observed[75,229]. Reasons for these large inter-laboratory discrepancies remain unclear and may have been linked to differences in analytical extraction protocols (for example, ^{14}C and ^{21}Ne), varying accuracy and precision of measurements of the stable isotopes, such as ^{27}Al measurements for the ^{26}Al technique, and the limited quality of reference materials (such as CRONUS-N[230]).

Repositories and reporting standards

Protocols for data reduction and analyses necessary to interpret cosmogenic nuclide data are continuously improved and updated, which in turn requires frequent recalculation of denudation rates, surface exposure and burial ages. Data reporting also depends critically on the standards underlying the measurements — most prominently, which AMS standard was used for the respective cosmogenic nuclide measurements[16]. Minimum reporting standards have been proposed in the past[231,232]; however, these are yet to be universally adopted. Metadata related to sample site location and characteristics (for example, latitude and longitude, elevation, topographic shielding, basin area) and to AMS standardization are necessary for the periodic recalculation of exposure ages and erosion rates as calculation procedures are refined. Although metadata such as procedural blank levels, raw AMS ratios, carrier amounts and concentrations are not needed in the recalculation of ages and rates, they are important to evaluate the quality of the actual measurements and, therefore, the quality and reliability of the calculated ages and erosion rates. Despite the lack of formalized and universally accepted reporting standards, the quality of data reporting has improved through time (FIG. 7). For example, more than 90% of ^{10}Be detrital denudation rate studies published between 2016 and 2020 ($n = 110$) report sufficient sample location metadata and usable AMS metadata. The recent improvements in cosmogenic nuclide reporting standards mirror similar developments in the wider scientific community towards better reporting of data[233]. Positive change has been spurred by the availability of easily accessible web-based exposure age and erosion rate calculators — such as the widely used platform labelled online calculators formerly known as the CRONUS-Earth online calculators[141] — that present users with rigid input and output data and metadata templates.

The past decade has witnessed numerous cosmogenic nuclide-based regional and global-scale synoptic studies[8,180,181,234] that have, ultimately, led to the creation of numerous curated global cosmogenic nuclide databases, including a global compilation of glacial ^{10}Be and ^{26}Al data, known as ExpAge; an open cosmogenic nuclide, luminescence and radiocarbon database known as OCTOPUS[154]; and ICE-D[16], a cosmogenic nuclide

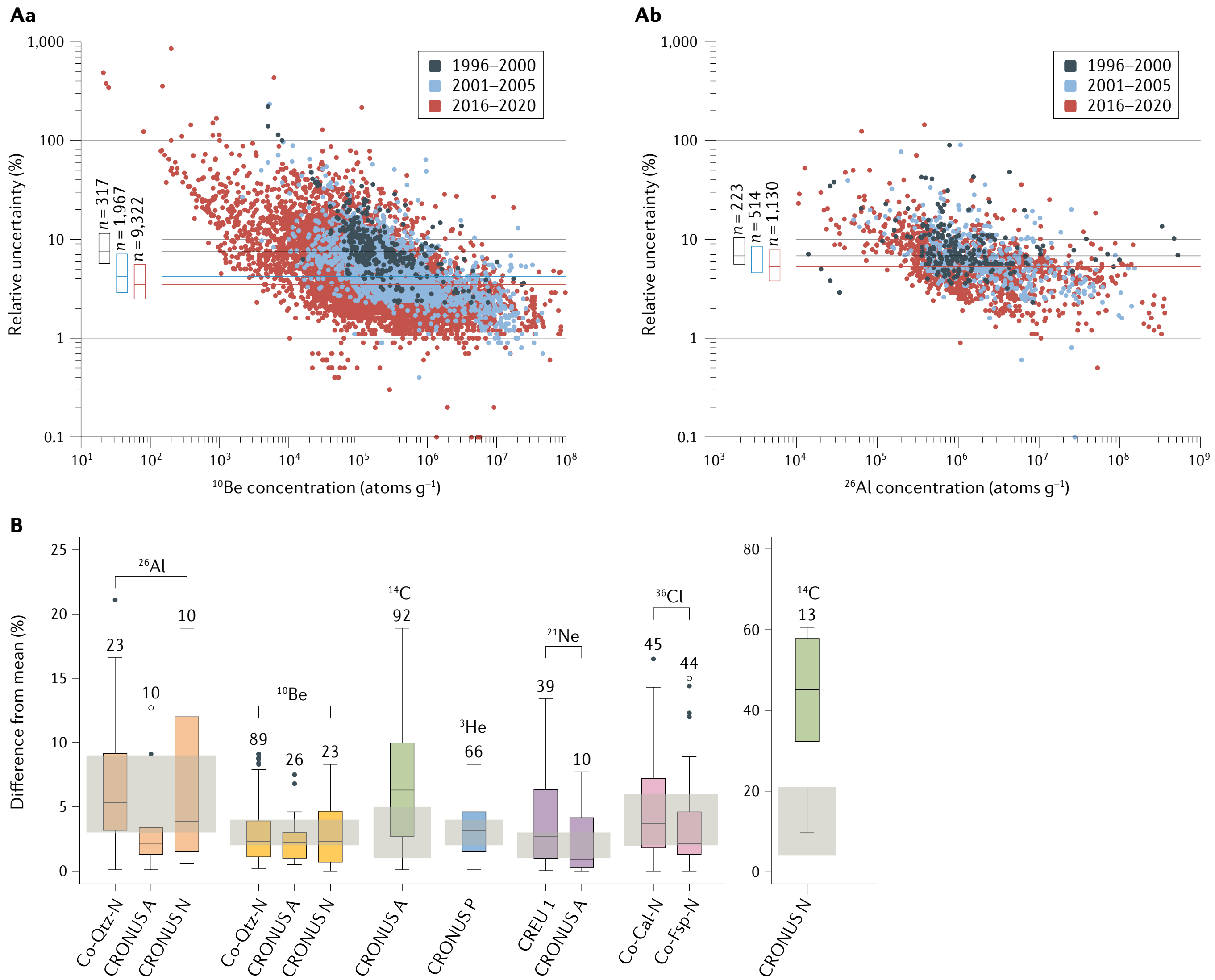

Fig. 6 | **Precision and accuracy of cosmogenic nuclide determinations. A** | Relative measurement accuracy versus ^{10}Be (part **Aa**) and ^{26}Al (part **Ab**) concentration for data published between 1996 and 2020. Box plots show median values and interquartile ranges. Data compiled from ExpAge — global compilation of glacial ^{10}Be and ^{26}Al data — and OCTOPUS databases. **B** | Compilation of laboratory inter-comparison reference material measurements. Nuclide concentrations normalized to mean values to allow comparison. Grey horizontal bands denote one standard deviation of nuclide measurement uncertainties. Data for ^{26}Al and ^{10}Be compiled from REFS[227,228], for ^{14}C from REFS[69,71,72,75,228,281], for ^{3}He from REF.[282], for ^{21}Ne from REF.[229] and for ^{36}Cl from REF.[283].

exposure age database, including data compilations and inter-comparison tools for ^{10}Be, ^{26}Al, ^{3}He and ^{21}Ne data from Antarctica, the Arctic and lower-latitude mountain glaciers[9].

Limitations and optimizations

Mineral separation and subsequent chemical isolation in the case of ^{10}Be and ^{26}Al remains an expensive and time-consuming process, and therefore is one of the main factors limiting sample size in any study. Sample preparation and chemistry procedures have changed little since their initial publication (for example, REFS[45,47,235]); however, there have been recent efforts to optimize[230,236,237] and even automate[238] beryllium and aluminium column chromatography. These efforts, however, fall short of the potential optimizations afforded by commercial automation solutions now employed for other isotopic systems[239–242]. Sample extraction also continues to be a major limitation for in situ ^{14}C applications[243], and several laboratories attempt to automatize to increase sample throughput and minimize opportunities for human error[70,71]. However, it is likely that major optimizations will result from the second generation of the simpler and more robust metal-based designs[72,75] that have already achieved lower blank levels[81], shorter extraction times and substantially improved reproducibility of standard materials[75].

Substantial improvements have been achieved in relation to the measurement of the various cosmogenic nuclides, including new and improved gas ion sources (in situ ^{14}C (REFS[100,101])), the use of a gas-filled magnet (^{26}Al and ^{36}Cl (REFS[244,245])), the use of ion–laser interaction

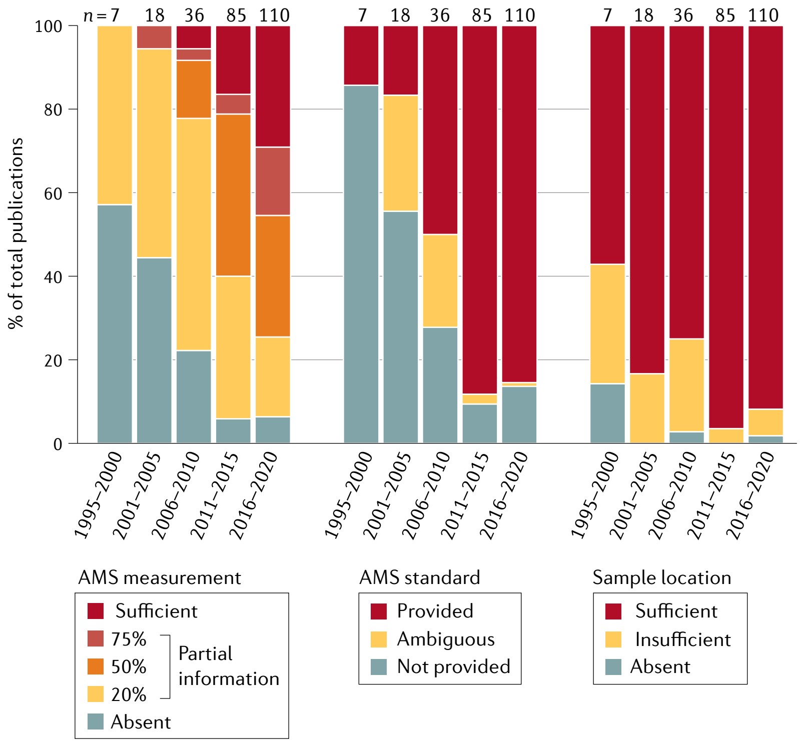

Fig. 7 | **Metadata reported in basin-wide cosmogenic ^{10}Be studies published between 1995 and 2020.** Accelerator mass spectrometry (AMS) measurement metadata: mass of quartz, mass of Be spike, AMS ratio, AMS standardization, value of blank or level of blank correction. Sufficient AMS measurement metadata include all five pieces of information. Sample location metadata: sample coordinates, basin area or outlet elevation, and map showing distribution of samples and basins. Sufficient location metadata occur with two or more pieces of information provided permit basin identification and re-delineation with confidence.

(^{36}Cl (REF.[245])) and new-generation instruments coming online (^{21}Ne (REF.[108])). Major limitations remain in relation to inter-laboratory discrepancies, as highlighted in FIG. 5 and discussed above.

Optimization of cosmogenic nuclide measurements improved sample throughput capacities, and large cosmogenic nuclide data sets afford tackling new scientific problems. For example, a deeper understanding of processes that control sediment production and transport at the catchment scale has been afforded by cosmogenic nuclide analyses from single-clast samples[216,246–249]. Large cosmogenic nuclide surface exposure age data sets allow for unambiguous identification of outliers[120], and data sets with large sample counts and numbers of measured cosmogenic nuclides have led to the development of more sophisticated numerical approaches to analyse them[216,250]. A further optimization has been the proliferation of exposure age and erosion rate calculators[141,142,179,251]. Although these have led to substantial improvements in data reporting and reproducibility (FIG. 7), the lack of clear standards for comparing cosmogenic nuclide-derived exposure ages and erosion rates with those obtained using other geochronometers remains a major limitation. Lastly, applications of meteoric ^{10}Be (REF.[252]) and of ^{36}Cl in magnetite[64] have extended the applicability of basin-wide denudation rate studies to non-quartz-bearing lithologies. This is a major improvement that will permit constraining the erosion and weathering rates of areas underlain by mafic and ultramafic rocks that exert an important control on regulating atmospheric CO_2 levels.

Outlook

The presented advances in cosmogenic nuclide techniques make it possible to ask new questions about the Earth and how it works, but building the capacity to answer them requires rising to an even bigger challenge: imbuing the cosmogenic nuclide discipline, and the geosciences as a whole, with a dedication to justice, equity, diversity and inclusion that matches our commitment to research.

New nuclides and new applications

The precision of AMS analyses of ^{10}Be, ^{26}Al and ^{36}Cl will further improve, which in turn will reduce the current uncertainties of the production rate ratios that are critical for many burial dating applications (FIG. 4). Similar is true for neon isotope measurements on the new generation of noble gas mass spectrometers. ATTA techniques are improving, opening new horizons for applications of, for example, ^{81}Kr. Laser trapping and cooling of neutral atoms has been realized on an increasing number of elements, including the alkali metals (Group I), alkaline earth metals (Group II) and noble gases. Whereas AMS can be used to analyse many different elements, an ATTA instrument is usually designed and built for only one specific element. For this reason, ATTA is best used to complement AMS, such as, for example, in the analysis of an isotope that is particularly challenging for AMS. Additional examples include ^{39}Ar (half-life of 269 days) and ^{41}Ca (half-life of 100 kyr), both nuclides with high potential that cannot be routinely analysed with AMS with sufficient sensitivity for geoscience applications.

Improvements in ATTA are allowing increased sensitivity for more cosmogenic nuclides of interest; ^{39}Ar is on the cusp of addressing major questions related to ocean circulation, one of the key elements of the Earth's system that is influenced by accelerating climate change[253]. The timescale of ocean circulation matches well with the half-life of ^{39}Ar. Therefore, a systematic ^{39}Ar dating programme of water mass transport throughout the ocean, in combination with ^{14}C data, is promising for high-resolution mapping of ocean currents, ocean mixing and deep-water formation rates, which are critical to evaluate the climate change-induced changes in ocean circulation, understanding sea level rise[254] and the capacity of the ocean to take up carbon dioxide[33,36,255,256].

Direct dating of old polar ice can provide critical insight into the stability of Earth's remaining ice sheets. Instead of producing metastable krypton atoms in a plasma, which inevitably leads to sample loss and contamination, a recent experiment has demonstrated optical excitation of ^{81}Kr to metastable level via a resonant vacuum ultraviolet lamp, followed by laser trapping and detection. The all-optical approach overcomes the limitations on precision and sample size of ^{81}Kr dating[257]. Dating of old polar ice with a 1 kg sample appears feasible.

Box 1 | **Justice, equity, diversity and inclusion**

In contrast to the substantial advances in analytical and methodological techniques, the cosmogenic community has struggled to bring a range of perspectives into our field, hindering intellectual progress on critical earth system questions[264]. Here we outline seven principles, drawn from the literature, that the cosmogenic nuclide community can use to improve the field.

- Respect — honour indigenous land and work with local communities to ensure there is mutual understanding, respect and trust[42,43,284].
- Recognition — only 28.5% of research excellence prizes awarded at the Swiss Geoscience Meeting were given to women over the period 2003 to 2019, a problem that is widespread within the discipline[266].
- Engagement — the majority of geoscience research articles on African topics have no African authors. Parachute research can further exacerbate inequities and illuminates a clear need for more intentional collaboration and inclusion of communities that are local to an area being studied[285].
- Leadership — geoscientists in China make up 25% of the authors, reviewers and editors for journals of the American Geophysical Union (AGU), the world's largest professional geoscience organization, and hold 2% of the leadership positions within the organization. By contrast, geoscientists in the United States make up 28% of authors, reviewers and editors yet hold 75% of leadership positions[286].
- Advancement — in Australasia, gender is still on the agenda in geosciences: at the professor level, women make up between 4 and 26% of each subdiscipline, and 6 of 11 sub-disciplines have fewer than 10% full professors who are women[265].
- Safety — remote fieldwork is particularly dangerous for geoscientists with marginalized identities[287].
- Intersectionality — in addition to fieldwork, the culture of geoscience in general can be particularly dangerous for geoscientists with multiple marginalized identities, making it critical to consider diversity not along a singular axis of oppression but with a full understanding of social and historical processes that influence who has access to geoscience[288,289].

Building a better community

Geoscientists share an appreciation for Earth, but despite this inherent connection to our planet, not everyone has equal access to its study. The earliest understandings of how our planet works emerged alongside violent histories of colonization, extraction and displacement[258], and the consequences of this legacy are apparent in the discipline today[259]. Overall, the field of cosmogenic nuclides has been dominated by European and American researchers; and even within these privileged groups, racism, misogyny and other violent forms of discrimination limit who can participate in the field. Ultimately, the outlook for cosmogenic nuclide geosciences depends on our ability, within our own communities and globally, to broaden participation such that everyone has access to understanding and contribution to the study of the Earth.

Many geoscientists have studied, discussed and advocated strategies for broadening participation in the discipline[260–262]. Here, we have identified seven principles that the cosmogenic nuclide community specifically can use to chart a course for a more just future: intersectionality, recognition, leadership, respect, engagement, advancement and safety. Each principle is broadly applicable, but we draw on the published literature to illustrate discrete examples (BOX 1).

Most disciplines fall short when it comes to equity, diversity and inclusion[263]. The deleterious impacts of these shortcomings are heightened in geoscience, including cosmogenic nuclide geoscience, because the status quo leads to real harm. For example, gender harassment is a well-documented manifestation of harm that both emerges from and exacerbates homogeneity. Gender harassment can take place in the classroom or laboratory, but can be particularly acute in the field settings where geoscientists, including cosmogenic nuclide geoscientists, work. Field settings are both a nucleus of harm in the geosciences and an area where targeted interventions can have cascading positive impacts on creating a more just community. As mentioned previously, using Indigenous research frameworks facilitates inclusive and transparent communication between different groups with a connection to the landscape, be it scientific, cultural, spiritual or a combination of these[43]. Such techniques take time, reflection, relationship-building and accountability to implement[43], but are crucial for moving the discipline away from our extractive roots[258] and towards a more just future[42]. Moreover, geoheritage and field-based ethno-geological research enhance our understanding of geological systems while promoting culturally informed teaching and research practices that serve under-represented cultural communities[264]. Taken together, these examples illuminate the critical need for a shared ethic, not only around fieldwork but in terms of intentionally creating structures that support cosmogenic nuclide geoscientists who are most likely to experience harm in their pursuit of new knowledge about the Earth.

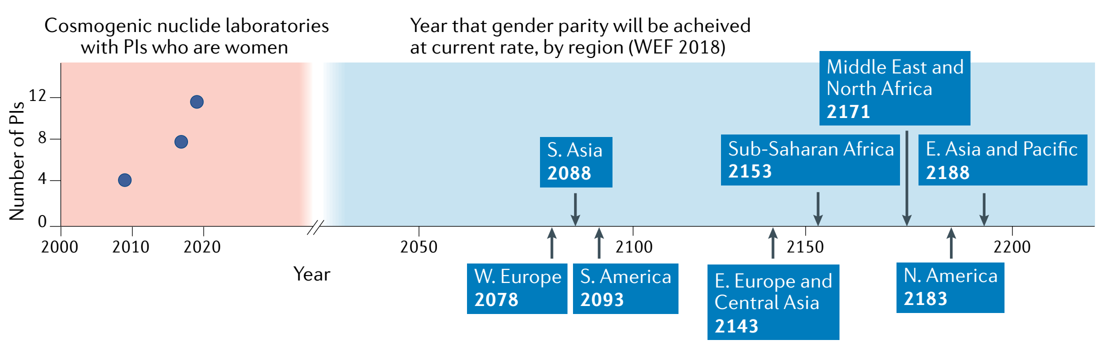

Fig. 8 | **Timeline of gender parity in cosmogenic nuclide geosciences.** Over the past decade, the number of cosmogenic nuclide laboratories with female Principal Investigators (PIs) has increased threefold from 4 in 2008 to 12 in 2020. If rates of change towards gender parity are not increased, it will take many decades to achieve gender parity within the broader field. Estimated date that each region will reach parity according to the World Economic Forum (WEF) is annotated along the timeline.

Although the field clearly has a long way to go, there has never been a more diverse cohort of aspiring geoscientists entering the field (AGI Currents 2020). Around the world, a robust pipeline exists for bringing more historically excluded groups into the discipline and building a community where everyone can participate fully, a clear necessity if we are going to rise to the challenge of addressing the most pressing geoscience problems that cosmogenic nuclide applications can solve[265,266]. However, at current rates of change, it will be many decades until gender parity is achieved in cosmogenic nuclide geosciences around the world (FIG. 8). In order to build a better community, we must embrace our commitment to justice, equity, diversity and inclusion with equal vigour to our study of the Earth.

Published online: 10 March 2022

1. Davis, R. J. & Schaeffer, O. A. Chlorine-36 in nature. *Ann. N.Y. Acad. Aci.* **62**, 105–122 (1955).
2. Suter, M. et al. Precision-measurements of C-14 in AMS — some results and prospects. *Nucl Instrum Methods Phys Res B* **5**, 117–122 (1984).
3. Graf, T., Kohl, C. P., Marti, K. & Nishiizumi, K. Cosmic-ray produced neon in antarctic rocks. *Geophys. Res. Lett.* **18**, 203–206 (1991).
4. Kurz, M. D. Cosmogenic helium in a terrestrial igneous rock. *Nature* **320**, 435–439 (1986).
5. Lal, D. Cosmic ray labeling of erosion surfaces: in situ nuclide production rates and erosion models. *Earth Planet. Sci. Lett.* **104**, 424–439 (1991).
6. Nishiizumi, K., Lal, D., Klein, R., Middleton, R. & Arnold, J. R. Production of ^{10}Be and ^{26}Al by cosmic rays in terrestrial quartz in situ and implications for erosion rates. *Nature* **319**, 134–136 (1986).
7. Phillips, F. M., Leavy, B. D., Jannik, N. O., Elmore, D. & Kubik, P. W. The accumulation pf cosmogenic Cl-36 in rocks — a method for surface exposure dating. *Science* **231**, 41–43 (1986).
8. Balco, G. Contributions and unrealized potential contributions of cosmogenic-nuclide exposure dating to glacier chronology, 1990–2010. *Quat. Sci. Rev.* **30**, 3–27 (2011).
9. Balco, G. Glacier change and paleoclimate applications of cosmogenic-nuclide exposure dating. *Annu. Rev. Earth Planet. Sci.* **48**, 21–48 (2020).
10. Cerling, T. E. & Craig, H. Geomorphology and in-situ cosmogenic isotopes. *Annu. Rev. Earth Planet. Sci.* **22**, 273–317 (1994).
11. Gosse, J. C. & Phillips, F. M. Terrestrial in situ cosmogenic nuclides: theory and application. *Quat. Sci. Rev.* **20**, 1475–1560 (2001).
12. Kurz, M. D. & Brook, E. J. in *Dating in Exposed and Surface Contexts* (ed. Beck, C.) 139–159 (Univ. New Mexico Press, 1994).
13. Blard, P. H., Bourles, D., Lave, J. & Pik, R. Applications of ancient cosmic-ray exposures: theory, techniques and limitations. *Quat. Geochronol.* **1**, 59–73 (2006).
14. Brown, L., Klein, J., Middleton, R., Sacks, I. S. & Tera, F. BE-10 in island-arc volcanos and implications for subduction. *Nature* **299**, 718–720 (1982).
15. Ivy-Ochs, S., Schlüchter, C., Prentice, M., Kubik, P. W. & Beer, J. ^{10}Be and ^{26}Al exposure ages for the Sirius Group at Mt. Fleming, Mt. Feather and the plateau surface at Table Mt. *The Antarctic Region: Geological Evolution and Processes* https://www.dora.lib4ri.ch/eawag/islandora/object/eawag:4487 (1997).
16. Balco, G. Technical note: A prototype transparent-middle-layer data management and analysis infrastructure for cosmogenic-nuclide exposure dating. *Geochronology* **2**, 169–175 (2020).
17. Putnam, A. E., Bromley, G. R. M., Rademaker, K. & Schaefer, J. M. In situ Be-10 production-rate calibration from a C-14-dated late-glacial moraine belt in Rannoch Moor, central Scottish Highlands. *Quat. Geochronol.* **50**, 109–125 (2019).
18. Granger, D. E. & Muzikar, P. F. Dating sediment burial with in situ-produced cosmogenic nuclides: theory, techniques, and limitations. *Earth Planet. Sci. Lett.* **188**, 269–281 (2001).
19. Corbett, L. B. et al. Cosmogenic Al-26/Be-10 surface production ratio in Greenland. *Geophys. Res. Lett.* **44**, 1350–1359 (2017).
20. Balco, G. & Shuster, D. L. Al-26–Be-10–Ne-21 burial dating. *Earth Planet. Sci. Lett.* **286**, 570–575 (2009).
21. Granger, D. E. A review of burial dating methods using Al-26 and Be-10. *Geol. Soc. Am.* https://doi.org/10.1130/2006.2415(01) (2006).
22. Nishiizumi, K. Preparation of Al-26 AMS standards. *Nucl. Instrum. Methods Phys. Res. Sect. B-Beam Interact. Mater. At.* **223**, 388–392 (2004).
23. Chmeleff, J., von Blanckenburg, F., Kossert, K. & Jakob, D. Determination of the Be-10 half-life by multicollector ICP-MS and liquid scintillation counting. *Nucl. Instrum. Methods Phys. Res. Sect. B Beam Interact. Mater. At.* **268**, 192–199 (2010).
24. Korschinek, G. et al. A new value for the half-life of Be-10 by heavy-ion elastic recoil detection and liquid scintillation counting. *Nucl. Instrum. Methods Phys. Res. Sect. B Beam Interact. Mater. At.* **268**, 187–191 (2010).
25. von Blanckenburg, F. The control mechanisms of erosion and weathering at basin scale from cosmogenic nuclides in river sediment. *Earth Planet. Sci. Lett.* **237**, 462–479 (2005).
26. Willenbring, J. K. & von Blanckenburg, F. Long-term stability of global erosion rates and weathering during late-Cenozoic cooling. *Nature* **465**, 211–214 (2010).
27. Willenbring, J. K. & von Blanckenburg, F. Meteoric cosmogenic beryllium-10 adsorbed to river sediment and soil: applications for Earth-surface dynamics. *Earth Sci. Rev.* **98**, 105–122 (2010).
28. Wittmann, H., Malusa, M. G., Resentini, A., Garzanti, E. & Niedermann, S. The cosmogenic record of mountain erosion transmitted across a foreland basin: source-to-sink analysis of in situ Be-10, Al-26 and Ne-21 in sediment of the Po river catchment. *Earth Planet. Sci. Lett.* **452**, 258–271 (2016).
29. Wittmann, H., von Blanckenburg, F., Maurice, L., Guyot, J. L. & Kubik, P. W. Recycling of Amazon floodplain sediment quantified by cosmogenic Al-26 and Be-10. *Geology* **39**, 467–470 (2011).
30. Beer, J. et al. Information on past solar activity and geomagnetism from ^{10}Be in the Camp Century ice core. *Nature* **331**, 675–679 (1988).
31. Loosli, H. H. & Oeschger, H. ^{37}Ar and ^{81}Kr in the atmosphere. *Earth Planet. Sci. Lett.* **7**, 67–78 (1969).
32. Loosli, H. H. A dating method with Ar-39. *Earth Planet. Sci. Lett.* **63**, 51–62 (1983).
33. Lu, Z. T. et al. Tracer applications of noble gas radionuclides in the geosciences. *Earth Sci. Rev.* **138**, 196–214 (2014).
34. Tian, L. et al. Kr-81 dating at the guliya ice cap, Tibetan Plateau. *Geophys. Res. Lett.* **46**, 6636–6643 (2019).
35. Buizert, C. et al. Greenland temperature response to climate forcing during the last deglaciation. *Science* **345**, 1177–1180 (2014).
36. Broecker, W. S. & Peng, T.-H. Comparison of ^{39}Ar and ^{14}C ages for waters in the deep ocean. *Nucl. Instrum. Methods Phys. Res. B* **172**, 473–478 (2000).
37. Moore, A. K., Granger, D. E. & Conyers, G. Beryllium cycling through deciduous trees and implications for meteoric ^{10}Be systematics. *Chem. Geol.* **571**, 120174 (2021).
38. Phillips, F. M. et al. The CRONUS-Earth Project: a synthesis. *Quat. Geochronol.* **31**, 119–154 (2016).
39. Kurz, M. D. In situ production of terrestrial cosmogenic helium and some applications to geochronology. *Geochim. Cosmochim. Acta* **50**, 2855–2862 (1986).
40. Butler, R. Destructive sampling ethics. *Nat. Geosci.* **8**, 817–818 (2015).
41. Mogk, D. W. & Bruckner, M. Z. Geoethics training in the Earth and environmental sciences. *Nat. Rev. Earth Environ.* **1**, 81–83 (2020).
42. David-Chavez, D. M. & Gavin, M. C. A global assessment of Indigenous community engagement in climate research. *Environ. Res. Lett.* **13**, 123005 (2018).
43. Reano, D. Using Indigenous research frameworks in the multiple contexts of research, teaching, mentoring, and leading. *Qual. Rep.* **25**, 3902–3926 (2020).
44. Carroll, S. R. et al. The CARE principles for Indigenous Data Governance. *Data Sci. J.* **19**, 43 (2020).
45. Kohl, C. P. & Nishiizumi, K. Chemical isolation of quartz for measurement of in-situ-produced cosmogenic nuclides. *Geochim. Cosmochim. Acta* **56**, 3583–3587 (1992).
46. Mifsud, C., Fujioka, T. & Fink, D. Extraction and purification of quartz in rock using hot phosphoric acid for in situ cosmogenic exposure dating. *Nucl. Instrum. Methods Phys. Res. Sect. B: Beam Interact. Mater. At.* **294**, 203–207 (2013).
47. Stone, J. A rapid fusion method for separation of beryllium-10 from soils and silicates. *Geochem. Cosmochem. Acta* **62**, 555–561 (1998).
48. Schaefer, J. M. et al. High frequency Holocene glacier fluctuations in New Zealand differ from the northern signature. *Science* **324**, 622 (2009).
49. Synal, H.-A. Developments in accelerator mass spectrometry. *Int. J. Mass. Spectrom.* **349**, 192–202 (2013).
50. Wilcken, K. M. et al. SIRIUS performance: ^{10}Be, ^{26}Al and ^{36}Cl measurements at ANSTO. *Nucl. Instrum. Methods Phys. Res. B* **455**, 300–304 (2019).
51. Kober, F. et al. In situ cosmogenic ^{10}Be and ^{21}Ne in sanidine and in situ cosmogenic ^{3}He in Fe–Ti-oxide minerals. *Earth Planet. Sci. Lett.* **236**, 404–418 (2005).
52. Eaves, S. R. et al. Further constraint of the in situ cosmogenic Be-10 production rate in pyroxene and a viability test for late Quaternary exposure dating. *Quat. Geochronol.* **48**, 121–132 (2018).
53. Braucher, R., Blard, P. H., Benedetti, L. & Bourles, D. L. in *In Situ-Produced Cosmogenic Nuclides and Quantification of Geological Processes Vol. 415 Geological Society of America Special Papers* (eds AlonsoZarza, A. M. & Tanner, L. H.) 17–28 (Geological Society of America, 2006).
54. Stone, J. O., Allan, G. L., Fifield, L. K. & Cresswell, R. G. Cosmogenic chlorine-36 from calcium spallation. *Geochim.Cosmochim. Acta* **60**, 679–692 (1996).
55. Schimmelpfennig, I. et al. Calibration of cosmogenic ^{36}Cl production rates from Ca and K spallation in lava flows from Mt. Etna (38° N, Italy) and Payun-Matru (36° S, Argentina). *Geochim. Cosmochim. Acta* **75**, 2611–2632 (2011).
56. Schimmelpfennig, I. et al. Cl-36 production rate from K-spallation in the European Alps (Chironico landslide, Switzerland). *J. Quat. Sci.* **29**, 407–413 (2014).
57. Stone, J. O. H., Evans, J. M., Fifield, L. K., Allan, G. L. & Cresswell, R. G. Cosmogenic chlorine-36 production in calcite by muons. *Geoch. Cosmochim. Acta* **62f**, 433–454 (1997).
58. Herber, L. J. Separation of feldspar from quartz by flotation. *Am. Miner.* **54**, 1212–1215 (1969).
59. Sulaymonova, V. A. et al. Feldspar flotation as a quartz-purification method in cosmogenic nuclide dating: a case study of fluvial sediments from the Pamir. *MethodsX* **5**, 717–726 (2018).
60. Bromley, G. R. M. et al. Pyroxene separation by HF leaching and its impact on helium surface-exposure dating. *Quat. Geochronol.* **23**, 1–8 (2014).
61. Bruno, L. A. et al. Dating of Sirius Group tillites in the Antarctic Dry Valleys with cosmogenic ^{3}He and ^{21}Ne. *Earth Planet. Sci. Lett.* **147**, 37–54 (1997).
62. Balter-Kennedy, A., Bromley, G., Balco, G., Thomas, H. & Jackson, M. S. A 14.5-million-year record of East Antarctic Ice Sheet fluctuations from the central Transantarctic Mountains, constrained with cosmogenic He-3, Be-10, Ne-21, and Al-26. *Cryosphere* **14**, 2647–2672 (2020).
63. Moore, A. K. & Granger, D. E. Watershed-averaged denudation rates from cosmogenic ^{36}Cl in detrital magnetite. *Earth Planet. Sci. Lett.* **527**, 115761 (2019).
64. Moore, A. K. & Granger, D. E. Calibration of the production rate of cosmogenic ^{36}Cl from Fe. *Quat. Geochronol.* **51**, 87–98 (2019).
65. Lifton, N. A., Jull, A. J. T. & Quade, J. A new extraction technique and production rate estimate for in situ cosmogenic ^{14}C in quartz. *Geochim. Cosmochim. Acta* **65**, 1953–1969 (2001).

66. Roman, H. *Measurements of in-Situ Production of ^{14}C in SiO_2 Production Rates and Cross-Sections*. PhD thesis, McMaster University (1989).
67. Jull, A. J. T., Wilson, A. E., Burr, G. S., Toolin, L. J. & Donahue, D. J. Measurements of cosmogenic C-14 produced by spallation in high-altitude rocks. *Radiocarbon* **34**, 737–744 (1992).
68. Fülöp, R.-H. et al. Update on the performance of the SUERC in situ cosmogenic C-14 extraction line. *Radiocarbon* **52**, 1288–1294 (2010).
69. Goehring, B. M., Schimmelpfennig, I. & Schaefer, J. M. Capabilities of the Lamont–Doherty Earth Observatory in situ C-14 extraction laboratory updated. *Quat. Geochronol.* **19**, 194–197 (2014).
70. Goehring, B. M., Wilson, J. & Nichols, K. A fully automated system for the extraction of in situ cosmogenic carbon-14 in the Tulane University cosmogenic nuclide laboratory. *Nucl. Instrum. Methods Phys. Res. Sect. B Beam Interact. Mater. At.* **455**, 284–292 (2019).
71. Lifton, N., Goehring, B., Wilson, J., Kubley, T. & Caffee, M. Progress in automated extraction and purification of in situ C-14 from quartz: results from the Purdue in situ C-14 laboratory. *Nucl. Instrum. Methods Phys. Res. Sect. B Beam Interact. Mater. At.* **361**, 381–386 (2015).
72. Fülöp, R.-H. et al. The ANSTO–University of Wollongong in-situ ^{14}C extraction laboratory. *Nucl. Instrum. Methods Phys. Res. Sect. B: Beam Interact. Mater. At.* **438**, 207–213 (2019).
73. Hippe, K. et al. An update on in situ cosmogenic C-14 analysis at ETH Zurich. *Nucl. Instrum. Methods Phys. Res. Sect. B Beam Interact. Mater. At.* **294**, 81–86 (2013).
74. Sliz, M. U., Espic, C., Hofmann, B. A., Leya, I. & Szidat, S. An update on the performance of the in situ C-14 extraction line at the University of Bern. *Radiocarbon* **62**, 1371–1388 (2020).
75. Lupker, M. et al. In-situ cosmogenic C-14 analysis at ETH Zurich: characterization and performance of a new extraction system. *Nucl. Instrum. Methods Phys. Res. Sect. B Beam Interact. Mater. At.* **457**, 30–36 (2019).
76. Lupker, M. et al. Depth-dependence of the production rate of in situ C-14 in quartz from the Leymon High core, Spain. *Quat. Geochronol.* **28**, 80–87 (2015).
77. Goehring, B. et al. The Rhone Glacier was smaller than today for most of the Holocene. *Geology* **39**, 679–682 (2011).
78. Wirsig, C. et al. Combined cosmogenic Be-10, in situ C-14 and Cl-36 concentrations constrain Holocene history and erosion depth of Grueben glacier (CH). *Swiss J. Geosci.* **109**, 379–388 (2016).
79. Young, N. E. et al. In situ cosmogenic ^{10}Be–^{14}C–^{26}Al measurements from recently deglaciated bedrock as a new tool to decipher changes in Greenland Ice Sheet size. *Clim. Past.* **17**, 419–450 (2021).
80. Fülöp, R.-H. et al. Million-year lag times in a post-orogenic sediment conveyor. *Sci. Adv.* **6**, eaaz8845 (2020).
81. Hippe, K. et al. Cosmogenic in situ ^{14}C–^{10}Be reveals abrupt Late Holocene soil loss in the Andean Altiplano. *Nat. Commun.* **12**, 2546–2546 (2021).
82. Zappala, J. C., McLain, D., Mueller, P. & Steeb, J. L. Enhanced detection limits for radiokrypton analysis. *J. Radioanal. Nucl. Chem.* **326**, 1075–1079 (2020).
83. Dong, X.-Z. et al. Dual separation of krypton and argon from environmental samples for radioisotope dating. *Anal. Chem.* **91**, 13576–13581 (2019).
84. Jull, A. J. T. & Burr, G. S. in *Treatise on Geochemistry* 2nd edn (eds Holland, H. D. & Turekian, K. K.) 375–383 (Elsevier, 2014).
85. Bennett, C. L. et al. Radiocarbon dating using electrostatic accelerators — negative-ions provide key. *Science* **198**, 508–510 (1977).
86. Muller, R. A. Radioisotope dating with a cyclotron. *Science* **196**, 489–494 (1977).
87. Nelson, D. E., Korteling, R. G. & Stott, W. R. C-14 — direct detection at natural concentrations. *Science* **198**, 507–508 (1977).
88. Raisbeck, G. M., Yiou, F., Fruneau, M. & Loiseaux, J. M. BE-10 mass-spectrometry with a cyclotron. *Science* **202**, 215–217 (1978).
89. Turekian, K. K. et al. Measurement of BE-10 in manganese nodules using a tandem Van de Graaff accelerator. *Geophys. Res. Lett.* **6**, 417–420 (1979).
90. Hidy, A. J. et al. A new Be-7 AMS capability established at CAMS and the potential for large datasets. *Nucl. Instrum. Methods Phys. Res. Sect. B Beam Interact. Mater. At.* **414**, 126–132 (2018).
91. Rood, D. H., Brown, T. A., Finkel, R. C. & Guilderson, T. P. Poisson and non-Poisson uncertainty estimations of Be-10/Be-9 measurements at LLNL-CAMS. *Nucl. Instrum. Methods Phys. Res. Sect. B Beam Interact. Mater. At.* **294**, 426–429 (2013).
92. Rood, D. H., Hall, S., Guilderson, T. P., Finkel, R. C. & Brown, T. A. Challenges and opportunities in high-precision Be-10 measurements at CAMS. *Nucl. Instrum. Methods Phys. Res. Sect. B Beam Interact. Mater. At.* **268**, 730–732 (2010).
93. Fifield, L. K., Tims, S. G., Gladkis, L. G. & Morton, C. R. Al-26 measurements with Be-10 counting statistics. *Nucl. Instrum. Methods Phys. Res. Sect. B Beam Interact. Mater. At.* **259**, 178–183 (2007).
94. Braumann, S. M. et al. Holocene glacier change in the Silvretta Massif (Austrian Alps) constrained by a new Be-10 chronology, historical records and modern observations. *Quat. Sci. Rev.* **245**, 106493 (2020).
95. Paul, M. Separation of isobars with a gas-filled magnet. *Nucl. Instrum. Methods Phys. Res. Sect. B Beam Interact. Mater. At.* **52**, 315–321 (1990).
96. Granger, D. E. et al. New cosmogenic burial ages for Sterkfontein Member 2 Australopithecus and Member 5 Oldowan. *Nature* **522**, 85–88 (2015).
97. Argento, D. C., Stone, J. O., Fifield, L. K. & Tims, S. G. Chlorine-36 in seawater. *Nucl. Instrum. Methods Phys. Res. Sect. B Beam Interact. Mater. At.* **268**, 1226–1228 (2010).
98. Ramsey, C. B., Higham, T. & Leach, P. Towards high-precision AMS: progress and limitations. *Radiocarbon* **46**, 17–24 (2004).
99. Yang, B., Smith, A. M. & Long, S. Second generation laser-heated microfurnace for the preparation of microgram-sized graphite samples. *Nucl. Instrum. Methods Phys. Res. Sect. B-Beam Interact. Mater. At.* **361**, 363–371 (2015).
100. Melchert, J. O. et al. Exploring sample size limits of AMS gas ion source C-14 analysis at CologneAMS. *Radiocarbon* **61**, 1785–1793 (2019).
101. Wacker, L. et al. A versatile gas interface for routine radiocarbon analysis with a gas ion source. *Nucl. Instrum. Methods Phys. Res. Sect. B Beam Interact. Mater. At.* **294**, 315–319 (2013).
102. Fujioka, T. et al. In situ cosmogenic ^{53}Mn production rate from ancient low-denudation surface in tropic Brazil. *Nucl. Instrum. Methods Phys. Res. B* **268**, 1209–1213 (2010).
103. Schaefer, J. M. et al. Terrestrial ^{53}Mn — a new monitor of Earth surface processes. *Earth Planet. Sci. Lett.* **251**, 334–345 (2006).
104. Aldrich, L. T. & Nier, A. O. Variation of He-3 He-4 abundance ratio in natural sources of helium. *Phys. Rev.* **74**, 1225–1225 (1948).
105. Reynolds, J. H. High sensitivity mass spectrometer for noble gas analysis. *Rev. Sci. Instrum.* **27**, 928–934 (1956).
106. Niedermann, S. et al. Cosmic-ray-produced ^{21}Ne in terrestrial quartz: the neon inventory of Sierra Nevada quartz separates. *Earth Planet. Sci. Lett.* **125**, 341–355 (1994).
107. Niedermann, S., Graf, T. & Marti, K. Mass spectrometric identification of cosmic-ray-produced neon in terrestrial rocks with multiple neon components. *Earth Planet. Sci. Lett.* **118**, 65–73 (1993).
108. Ritter, B., Vogt, A. & Dunai, T. J. Technical Note: Noble gas extraction procedure and performance of the Cologne Helix MC Plus multi-collector noble gas mass spectrometer for cosmogenic neon isotope analysis. *Geochronol. Discuss.* **2021**, 1–16 (2021).
109. Renne, P. R., Farley, K. A., Becker, T. A. & Sharp, W. D. Terrestrial cosmogenic argon. *Earth Planet. Sci. Lett.* **188**, 435–440 (2001).
110. Niedermann, S., Schaefer, J. M., Wieler, R. & Naumann, R. The production rate of cosmogenic ^{38}Ar from calcium in terrestrial pyroxene. *Earth Planet. Sci. Lett.* **257**, 596–608 (2007).
111. Raab, E. L., Prentiss, M., Cable, A., Chu, S. & Pritchard, D. E. Trapping of neutral sodium atoms with radiation pressure. *Phys. Rev. Lett.* **59**, 2631–2634 (1987).
112. Granger, D. E., Lifton, N. A. & Willenbring, J. K. A cosmic trip: 25 years of cosmogenic nuclides in geology. *Geol. Soc. Am. Bull.* **125**, 1379–1402 (2013).
113. Putnam, A. E. et al. Glacier advance in southern middle-latitudes during the Antarctic Cold Reversal. *Nat. Geosci.* **3**, 700–704 (2010).
114. Spector, P. et al. Rapid early-Holocene deglaciation in the Ross Sea, Antarctica. *Geophys. Res. Lett.* **44**, 7817–7825 (2017).
115. Ullman, D. J. et al. Southern Laurentide ice-sheet retreat synchronous with rising boreal summer insolation. *Geology* **43**, 23–26 (2015).
116. Kelly, M. A. et al. Expanded glaciers during a dry and cold Last Glacial Maximum in equatorial East Africa. *Geology* **42**, 519–522 (2014).
117. Levy, L. B. et al. Coeval fluctuations of the Greenland Ice Sheet and a local glacier, central East Greenland, during late glacial and early Holocene time. *Geophys. Res. Lett.* **43**, 1623–1631 (2016).
118. Schaefer, J. M. et al. The Southern Glacial Maximum 65,000 years ago and its unfinished termination. *Quat. Sci. Rev.* **114**, 52–60 (2015).
119. Strand, P. D. et al. Millennial-scale pulsebeat of glaciation in the Southern Alps of New Zealand. *Quat. Sci. Rev.* **220**, 165–177 (2019).
120. Young, N. E. et al. Deglaciation of the Greenland and Laurentide ice sheets interrupted by glacier advance during abrupt coolings. *Quat. Sci. Rev.* **229**, 106091 (2020).
121. Zhang, Q. et al. Quaternary glaciations in the Lopu Kangri area, central Gangdise Mountains, southern Tibetan Plateau. *Quat. Sci. Rev.* **201**, 470–482 (2018).
122. Ivy-Ochs, S. et al. The timing of glacier advances in the northern European Alps based on surface exposure dating with cosmogenic Be-10, Al-26, Cl-36, and Ne-21. *GSA Spec. Pap.* **415**, 43–60 (2006).
123. Ivy-Ochs, S. et al. Chronology of the last glacial cycle in the European Alps. *J. Quat. Sci.* **23**, 559–573 (2008).
124. Larsen, N. K. et al. Holocene ice marginal fluctuations of the Qassimiut lobe in South Greenland. *Sci. Rep.* **6**, 22362 (2016).
125. Larsen, N. K. et al. Strong altitudinal control on the response of local glaciers to Holocene climate change in southwest Greenland. *Quat. Sci. Rev.* **168**, 69–78 (2017).
126. Levy, L. B. et al. Multi-phased deglaciation of south and southeast Greenland controlled by climate and topographic setting. *Quat. Sci. Rev.* **242**, 106454 (2020).
127. Claude, A. et al. The Chironico landslide (Valle Leventina, southern Swiss Alps): age and evolution. *Swiss J. Geosci.* **107**, 273–291 (2014).
128. Putnam, A. et al. In situ cosmogenic ^{10}Be production-rate calibration from the Southern Alps, New Zealand. *Quat. Geochronol.* **5**, 392–409 (2010).
129. Briner, J. P., Young, N. E., Goehring, B. & Schaefer, J. M. Constraining Holocene ^{10}Be production rates in Greenland. *J. Quat. Sci.* **27**, 2–6 (2012).
130. Fenton, C. R. et al. Regional ^{10}Be production rate calibration for the past 12 ka deduced from the radiocarbon-dated Grotlandsura and Russenes rock avalanches at 69° N, Norway. *Quat. Geochronol.* **6**, 437–452 (2011).
131. Young, N. E., Schaefer, J. M., Briner, J. P. & Goehring, B. M. A Be-10 production-rate calibration for the Arctic. *J. Quat. Sci.* **28**, 515–526 (2013).
132. Borchers, B. et al. Geological calibration of spallation production rates in the CRONUS-Earth Project. *Quat. Geochronol.* **31**, 188–198 (2016).
133. Schimmelpfennig, I. et al. Calibration of the in situ cosmogenic ^{14}C production rate in New Zealand's Southern Alps. *J. Quat. Sci.* **27**, 671–674 (2012).
134. Young, N. E. et al. West Greenland and global in situ C-14 production-rate calibrations. *J. Quat. Sci.* **29**, 401–406 (2014).
135. Fenton, C. R., Niedermann, S., Dunai, T. & Binnie, S. A. The SPICE project: production rates of cosmogenic Ne-21, Be-10, and C-14 in quartz from the 72 ka SP basalt flow, Arizona, USA. *Quat. Geochronol.* **54**, 101019 (2019).
136. Lal, D., Malhotra, P. K. & Peters, B. On the production of radioisotopes in the atmosphere by cosmic radiation and their application to meteorology. *J. Atmos. Terr. Phys.* **12**, 306–328 (1958).
137. Argento, D. C., Stone, J. O., Reedy, R. C. & O'Brien, K. Physics-based modeling of cosmogenic nuclides part I — radiation transport methods and new insights. *Quat. Geochronol.* **26**, 29–43 (2015).
138. Argento, D. C., Stone, J. O., Reedy, R. C. & O'Brien, K. Physics-based modeling of cosmogenic nuclides part II — key aspects of in-situ cosmogenic nuclide production. *Quat. Geochronol.* **26**, 44–55 (2015).
139. Lifton, N., Sato, T. & Dunai, T. J. Scaling in situ cosmogenic nuclide production rates using analytical approximations to atmospheric cosmic-ray fluxes. *Earth Planet. Sci. Lett.* **386**, 149–160 (2014).
140. Masarik, J. & Reedy, R. C. Terrestrial cosmogenic-nuclide production systematics calculated from numerical simulations. *Earth Planet. Sci. Lett.* **136**, 381–395 (1995).
141. Balco, G., Stone, J. O., Lifton, N. A. & Dunai, T. J. A complete and easily accessible means of calculating

surface exposure ages or erosion rates from Be-10 and Al-26 measurements. *Quat. Geochronol.* **3**, 174–195 (2008).
142. Marrero, S. M. et al. Cosmogenic nuclide systematics and the CRONUScalc program. *Quat. Geochronol.* **31**, 160–187 (2016).
143. Akçar, N. et al. The AD 1717 rock avalanche deposits in the upper Ferret Valley (Italy): a dating approach with cosmogenic ^{10}Be. *J. Quat. Sci.* **27**, 383–392 (2012).
144. Kaplan, M. et al. Patagonian and southern South Atlantic view of Holocene climate. *Quat. Sci. Rev.* **141**, 112–125 (2016).
145. Putnam, A. E. et al. Regional climate control of glaciers in New Zealand and Europe during the pre-industrial Holocene. *Nat. Geosci.* **5**, 627–630 (2012).
146. Reynhout, S. et al. Holocene glacier fluctuations in Patagonia are modulated by summer insolation intensity and paced by Southern Annular Mode-like variability. *Quat. Sci. Rev.* **220**, 178–187 (2019).
147. Schimmelpfennig, I. et al. Holocene glacier culminations in the Western Alps and their hemispheric relevance. *Geology* **40**, 891–894 (2012).
148. Eaves, S. R. et al. Late-glacial and Holocene glacier fluctuations in North Island, New Zealand. *Quat. Sci. Rev.* **223**, 105914 (2019).
149. Schimmelpfennig, I. et al. A chronology of Holocene and Little Ice Age glacier culminations of the Steingletscher, CentralAlps, Switzerland, based on high-sensitivity beryllium-10 moraine dating. *Earth Planet. Sci. Lett.* **393**, 220–230 (2014).
150. Halsted, C. T., Bierman, P. R. & Balco, G. Empirical evidence for latitude and altitude variation of the in situ cosmogenic ^{26}Al/^{10}Be production ratio. *Geosciences* **11**, 402 (2021).
151. Balco, G. Chlorine-36/beryllium-10 burial dating of alluvial fan sediments associated with the Mission Creek strand of the San Andreas Fault system, California, USA. *Geochronology* **1**, 1–16 (2019).
152. Goehring, B. M., Muzikar, P. & Lifton, N. A. An in situ ^{14}C–^{10}Be Bayesian isochron approach for interpreting complex glacial histories. *Quat. Geochronol.* **15**, 61–66 (2013).
153. Brown, L., Pavich, M. J., Hickman, R. E., Klein, J. & Middleton, R. Erosion of the eastern-United-States observed with Be-10. *Earth Surf. Process. Landf.* **13**, 441–457 (1988).
154. Codilean, A. T. et al. OCTOPUS: an open cosmogenic isotope and luminescence database. *Earth Syst. Sci. Data* **10**, 2123–2139 (2018).
155. Kirchner, J. W. et al. Mountain erosion over 10 yr, 10 k.y., and 10 m.y. time scales. *Geology* **29**, 591–594 (2001).
156. Riebe, C. S., Kirchner, J. W., Granger, D. E. & Finkel, R. C. Erosional equilibrium and disequilibrium in the Sierra Nevada, inferred from cosmogenic Al-26 and Be-10 in alluvial sediment. *Geology* **28**, 803–806 (2000).
157. Heimsath, A. M., Dietrich, W. E., Nishiizumi, K. & Finkel, R. C. The soil production function and landscape equilibrium. *Nature* **388**, 358–361 (1997).
158. Schaller, M. & Ehlers, T. A. Limits to quantifying climate driven changes in denudation rates with cosmogenic radionuclides. *Earth Planet. Sci. Lett.* **248**, 153–167 (2006).
159. Allen, P. A. From landscapes into geological history. *Nature* **451**, 274–276 (2008).
160. Cyr, A. J. & Granger, D. E. Dynamic equilibrium among erosion, river incision, and coastal uplift in the northern and central Apennines, Italy. *Geology* **36**, 103–106 (2008).
161. Grischott, R. et al. Millennial scale variability of denudation rates for the last 15 kyr inferred from the detrital Be-10 record of Lake Stappitz in the Hohe Tauern massif, Austrian Alps. *Holocene* **27**, 1914–1927 (2017).
162. Madella, A., Delunel, R., Akcar, N., Schlunegger, F. & Christl, M. Be-10-inferred paleo-denudation rates imply that the mid-Miocene western central Andes eroded as slowly as today. *Sci. Rep.* **8**, 2299 (2018).
163. Oskin, M. E. et al. Steady Be-10-derived paleoerosion rates across the Plio-Pleistocene climate transition, Fish Creek-Vallecito basin, California. *J. Geophys. Res. Earth Surf.* **122**, 1653–1677 (2017).
164. Gerber, C. et al. Using Kr-81 and noble gases to characterize and date groundwater and brines in the Baltic Artesian Basin on the one-million-year timescale. *Geochim. Cosmochim. Acta* **205**, 187–210 (2017).
165. Weber, N. et al. The circulation of the Dead Sea brine in the regional aquifer. *Earth Planet. Sci. Lett.* **493**, 242–261 (2018).
166. Yechieli, Y. et al. Recent seawater intrusion into deep aquifer determined by the radioactive noble-gas isotopes Kr-81 and Ar-39. *Earth Planet. Sci. Lett.* **507**, 21–29 (2019).
167. Ram, R. et al. Identifying recharge processes into a vast "fossil" aquifer based on dynamic groundwater Kr-81 age evolution. *J. Hydrol.* **587**, 124946 (2020).
168. Yokochi, R. et al. Radiokrypton unveils dual moisture sources of a deep desert aquifer. *Proc. Natl Acad. Sci. USA* **116**, 16222–16227 (2019).
169. Zhang, J. et al. Inflection points on groundwater age and geochemical profiles along wellbores light up hierarchically nested flow systems. *Geophys. Res. Lett.* **48**, e2020GL092337 (2021).
170. Aggarwal, P. K. et al. Continental degassing of He-4 by surficial discharge of deep groundwater. *Nat. Geosci.* **8**, 35–39 (2015).
171. Matsumoto, T. et al. Application of combined Kr-81 and He-4 chronometers to the dating of old groundwater in a tectonically active region of the North China Plain. *Earth Planet. Sci. Lett.* **493**, 208–217 (2018).
172. Matsumoto, T. et al. Krypton-81 dating of the deep Continental Intercalaire aquifer with implications for chlorine-36 dating. *Earth Planet. Sci. Lett.* **535**, 116120 (2020).
173. Buizert, C. et al. Radiometric Kr-81 dating identifies 120,000-year-old ice at Taylor Glacier, Antarctica. *Proc. Natl Acad. Sci. USA* **111**, 6876–6881 (2014).
174. Crotti, I. et al. An extension of the TALDICE ice core age scale reaching back to MIS 10.1. *Quat. Sci. Rev.* **266**, 107078 (2021).
175. Crotti, I. et al. New δ18Oatm, δ18Oice and δDice profiles from deep ice of the TALDICE core. *EGU General Assembly 2020* https://doi.org/10.5194/egusphere-egu2020-4179 (2020).
176. Dixon, J. L. & Riebe, C. S. Tracing and pacing soil across slopes. *Elements* **10**, 363–368 (2014).
177. Herman, F. et al. Worldwide acceleration of mountain erosion under a cooling climate. *Nature* **504**, 423–419 (2013).
178. Hippe, K. Constraining processes of landscape change with combined in situ cosmogenic C-14–Be-10 analysis. *Quat. Sci. Rev.* **173**, 1–19 (2017).
179. Mudd, S. M., Harel, M.-A., Hurst, M. D., Grieve, S. W. D. & Marrero, S. M. The CAIRN method: automated, reproducible calculation of catchment-averaged denudation rates from cosmogenic nuclide concentrations. *Earth Surf. Dyn.* **4**, 655–674 (2016).
180. Portenga, E. W. & Bierman, P. R. Understanding Earth's eroding surface with ^{10}Be. *GSA Today* **21**, 4–10 (2011).
181. Willenbring, J. K., Codilean, A. T. & McElroy, B. Earth is (mostly) flat: apportionment of the flux of continental sediment over millennial time scales. *Geology* **41**, 343–346 (2013).
182. Harel, M. A., Mudd, S. M. & Attal, M. Global analysis of the stream power law parameters based on worldwide Be-10 denudation rates. *Geomorphology* **268**, 184–196 (2016).
183. Ben-Israel, M., Matmon, A., Hidy, A. J., Avni, Y. & Balco, G. Early-to-mid Miocene erosion rates inferred from pre-Dead Sea rift Hazeva River fluvial chert pebbles using cosmogenic Ne-21. *Earth Surf. Dyn.* **8**, 289–301 (2020).
184. Rosenkranz, R., Schildgen, T., Wittmann, H. & Spiegel, C. Coupling erosion and topographic development in the rainiest place on Earth: Reconstructing the Shillong Plateau uplift history with in-situ cosmogenic Be-10. *Earth Planet. Sci. Lett.* **483**, 39–51 (2018).
185. Brocard, G. Y., Willenbring, J. K., Miller, T. E. & Scatena, F. N. Relict landscape resistance to dissection by upstream migrating knickpoints. *J. Geophys. Res. Earth Surf.* **121**, 1182–1203 (2016).
186. Hewawasam, T., von Blanckenburg, F., Schaller, M. & Kubik, P. Increase of human over natural erosion rates in tropical highlands constrained by cosmogenic nuclides. *Geology* **31**, 597–600 (2003).
187. Bekaddour, T. et al. Paleo erosion rates and climate shifts recorded by Quaternary cut-and-fill sequences in the Pisco Valley, central Peru. *Earth Planet. Sci. Lett.* **390**, 103–115 (2014).
188. Fuller, T. K., Perg, L. A., Willenbring, J. K. & Lepper, K. Field evidence for climate-driven changes in sediment supply leading to strath terrace formation. *Geology* **37**, 467–470 (2009).
189. Garcin, Y. et al. Short-lived increase in erosion during the African Humid Period: evidence from the northern Kenya Rift. *Earth Planet. Sci. Lett.* **459**, 58–69 (2017).
190. Grischott, R. et al. Constant denudation rates in a high alpine catchment for the last 6 kyrs. *Earth Surf. Process. Landf.* **42**, 1065–1077 (2017).
191. Marshall, J. A., Roering, J. J., Gavin, D. G. & Granger, D. E. Late Quaternary climatic controls on erosion rates and geomorphic processes in western Oregon, USA. *Geol. Soc. Am. Bull.* **129**, 715–731 (2017).
192. Schaller, M. et al. A 30 000 yr record of erosion rates from cosmogenic Be-10 in Middle European river terraces. *Earth Planet. Sci. Lett.* **204**, 307–320 (2002).
193. Haeuselmann, P., Granger, D. E., Jeannin, P. Y. & Lauritzen, S. E. Abrupt glacial valley incision at 0.8 Ma dated from cave deposits in Switzerland. *Geology* **35**, 143–146 (2007).
194. Mason, C. C. & Romans, B. W. Climate-driven unsteady denudation and sediment flux in a high-relief unglaciated catchment-fan using Al-26 and Be-10: Panamint Valley, California. *Earth Planet. Sci. Lett.* **492**, 130–143 (2018).
195. Pingel, H., Schildgen, T., Strecker, M. R. & Wittmann, H. Pliocene–Pleistocene orographic control on denudation in northwest Argentina. *Geology* **47**, 359–362 (2019).
196. Balco, G. & Stone, J. O. H. Measuring middle Pleistocene erosion rates with cosmic-ray-produced nuclides in buried alluvial sediment, Fisher Valley, southeastern Utah. *Earth Surf. Process. Landf.* **30**, 1051–1067 (2005).
197. Val, P., Hoke, G. D., Fosdick, J. C. & Wittmann, H. Reconciling tectonic shortening, sedimentation and spatial patterns of erosion from ^{10}Be paleo-erosion rates in the Argentine Precordillera. *Earth Planet. Sci. Lett.* **450**, 173–185 (2016).
198. Puchol, N. et al. Limited impact of Quaternary glaciations on denudation rates in Central Asia. *Geol. Soc. Am. Bull.* **129**, 479–499 (2017).
199. Charreau, J. et al. Paleo-erosion rates in Central Asia since 9 Ma: a transient increase at the onset of Quaternary glaciations? *Earth Planet. Sci. Lett.* **304**, 85–92 (2011).
200. Mariotti, A. et al. Nonlinear forcing of climate on mountain denudation during glaciations. *Nat. Geosci.* **14**, 16–22 (2021).
201. Masson-Delmotte, V. et al. in *Global Warming of 1.5 °C. An IPCC Special Report on the impacts of global warming of 1.5 °C above pre-industrial levels and related global greenhouse gas emission pathways, in the context of strengthening the global response to the threat of climate change, sustainable development, and efforts to eradicate poverty* 32 (World Meteorological Organization, 2018).
202. Tedesco, M. & Fettweis, X. Unprecedented atmospheric conditions (1948–2019) drive the 2019 exceptional melting season over the Greenland Ice Sheet. *Cryosphere* **14**, 1209–1223 (2020).
203. Sasgen, I. et al. Return to rapid ice loss in Greenland and record loss in 2019 detected by the GRACE-FO satellites. *Commun. Earth Environ.* **1**, 8 (2020).
204. Briner, J. P. et al. Rate of mass loss from the Greenland Ice Sheet will exceed Holocene values this century. *Nature* **586**, 70–74 (2020).
205. Larsen, N. K. et al. The response of the southern Greenland Ice Sheet to the Holocene thermal maximum. *Geology* **43**, 291–294 (2015).
206. Beel, C. R., Lifton, N. A., Briner, J. P. & Goehring, B. M. Quaternary evolution and ice sheet history of contrasting landscapes in Uummannaq and Sukkertoppen, western Greenland. *Quat. Sci. Rev.* **149**, 248–258 (2016).
207. Briner, J. P. et al. Holocene climate change in Arctic Canada and Greenland. *Quat. Sci. Rev.* **147**, 340–364 (2016).
208. Kelly, M. A. et al. A ^{10}Be chronology of lateglacial and Holocene mountain glaciation in the Scoresby Sund region, east Greenland: implications for seasonality during lateglacial time. *Quat. Sci. Rev.* **27**, 2273–2282 (2008).
209. Bierman, P. R. et al. Preservation of a preglacial landscape under the center of the Greenland Ice Sheet. *Science* **344**, 402–405 (2014).
210. Bierman, P. R., Shakun, J. D., Corbett, L. B., Zimmerman, S. R. & Rood, D. H. A persistent and dynamic East Greenland Ice Sheet over the past 7.5 million years. *Nature* **540**, 256–260 (2016).
211. Yau, A. M., Bender, M. L., Blunier, T. & Jouzel, J. Setting a chronology for the basal ice at Dye-3 and GRIP: implications for the long-term stability of the Greenland Ice Sheet. *Earth Planet. Sci. Lett.* **451**, 1–9 (2016).
212. NEEM community members. Eemian interglacial reconstructed from a Greenland folded ice core. *Nature* **493**, 489–494 (2013).
213. Schaefer, J. M. et al. Greenland was nearly ice-free for extended periods during the Pleistocene. *Nature* **540**, 252–255 (2016).

214. Christ, A. J. et al. A multimillion-year-old record of Greenland vegetation and glacial history preserved in sediment beneath 1.4 km of ice at Camp Century. *Proc. Natl Acad. Sci. USA* **118**, e2021442118 (2021).
215. Voosen, P. Greenland rock cores to trace ice's past melting. *Science* **369**, 19 (2020).
216. Prush, V. B. & Oskin, M. E. A mechanistic erosion model for cosmogenic nuclide inheritance in single-clast exposure ages. *Earth and Planet. Sci. Lett.* **535**, 116066 (2020).
217. Balco, G., Purvance, M. D. & Rood, D. H. Exposure dating of precariously balanced rocks. *Quat. Geochronol.* **6**, 295–303 (2011).
218. Rood, A. H. et al. Earthquake hazard uncertainties improved using precariously balanced rocks. *AGU Adv.* **1**, e2020AV000182 (2020).
219. Soldati, M., Barrows, T. T., Prampolini, M. & Fifield, K. L. Cosmogenic exposure dating constraints for coastal landslide evolution on the Island of Malta (Mediterranean Sea). *J. Coast. Conserv.* **22**, 831–844 (2018).
220. Hurst, M. D., Rood, D. H., Ellis, M. A., Anderson, R. S. & Dornbusch, U. Recent acceleration in coastal cliff retreat rates on the south coast of Great Britain. *Proc. Natl Acad. Sci. USA* **113**, 13336–13341 (2016).
221. Ramalho, R. S. et al. Hazard potential of volcanic flank collapses raised by new megatsunami evidence. *Sci. Adv.* **1**, e1500456 (2015).
222. Tremblay, M. M., Shuster, D. L., Balco, G. & Cassata, W. S. Neon diffusion kinetics and implications for cosmogenic neon paleothermometry in feldspars. *Geochim. Cosmochim. Acta* **205**, 14–30 (2017).
223. Zeitler, P. K. & Tremblay, M. M. Measuring noble gases for thermochronology. *Elements* **16**, 343–345 (2020).
224. Tremblay, M. M. & Cassata, W. S. Noble gas thermochronology of extraterrestrial materials. *Elements* **16**, 331–336 (2020).
225. Clarke, R. J., Partridge, T. C., Granger, D. E. & Caffe, M. W. Dating the Sterkfontein fossils. *Science* **301**, 596–597 (2003).
226. Stuart, F. M. & Dunai, T. J. Editorial. *Quat. Geochronol.* **4**, 435–436 (2009).
227. Binnie, S. A. et al. Preliminary results of CoQtz-N: a quartz reference material for terrestrial in situ cosmogenic Be-10 and Al-26 measurements. *Nucl. Instrum. Methods Phys. Res. Sect. B Beam Interact. Mater. At.* **456**, 203–212 (2019).
228. Jull, A. J. T., Scott, E. M. & Bierman, P. The CRONUS-Earth inter-comparison for cosmogenic isotope analysis. *Quat. Geochronol.* **26**, 3–10 (2015).
229. Vermeesch, P. et al. Interlaboratory comparison of cosmogenic ^{21}Ne in quartz. *Quat. Geochronol.* **26**, 20–28 (2015).
230. Corbett, L. B., Bierman, P. R., Woodruff, T. E. & Caffee, M. W. A homogeneous liquid reference material for monitoring the quality and reproducibility of in situ cosmogenic ^{10}Be and ^{26}Al analyses. *Nucl. Instrum. Methods Phys. Res. Sect. B: Beam Interact. Mater. At.* **456**, 180–185 (2019).
231. Dunai, T. J. & Stuart, F. M. Reporting of cosmogenic nuclide data for exposure age and erosion rate determinations. *Quat. Geochronol.* **4**, 437–440 (2009).
232. Frankel, K. L., Finkel, R. C. & Owen, L. A. Terrestrial cosmogenic nuclide geochronology data reporting standards needed. *EOS Trans. AGU* **91**, 31–32 (2010).
233. Wilkinson, M. D. et al. Comment: the FAIR Guiding Principles for scientific data management and stewardship. *Sci. Data* **3**, 160018 (2016).
234. Heyman, J. Paleoglaciation of the Tibetan Plateau and surrounding mountains based on exposure ages and ELA depression estimates. *Quat. Sci. Rev.* **91**, 30–41 (2014).
235. Blanckenburg, F. V., Belshaw, N. S. & O'Nions, R. K. Separation of Be-9 and cosmogenic Be-10 from environmental materials and SIMS isotope dilution analysis. *Chem. Geol.* **129**, 93–99 (1996).
236. Binnie, S. A. et al. Separation of Be and Al for AMS using single-step column chromatography. *Nucl. Instrum. Methods Phys. Res. Sect. B Beam Interact. Mater. At.* **361**, 397–401 (2015).
237. Corbett, L. B., Bierman, P. R. & Rood, D. H. An approach for optimizing in situ cosmogenic Be-10 sample preparation. *Quat. Geochronol.* **33**, 24–34 (2016).
238. Keddadouche, K. et al. Design and performance of an automated chemical extraction bench for the preparation of Be-10 and Al-26 targets to be analyzed by accelerator mass spectrometry. *Nucl. Instrum. Methods Phys. Res. Sect. B Beam Interact. Mater. At.* **456**, 230–235 (2019).
239. Enge, T. G. et al. An automated chromatography procedure optimized for analysis of stable Cu isotopes from biological materials. *J. Anal. At. Spectrom.* **31**, 2023–2030 (2016).
240. Retzmann, A., Zimmermann, T., Pröfrock, D., Prohaska, T. & Irrgeher, J. A fully automated simultaneous single-stage separation of Sr, Pb, and Nd using DGA Resin for the isotopic analysis of marine sediments. *Anal. Bioanal. Chem.* **409**, 5463–5480 (2017).
241. Wefing, A.-M. et al. High precision U-series dating of scleractinian cold-water corals using an automated chromatographic U and Th extraction. *Chem. Geol.* **475**, 140–148 (2017).
242. Romaniello, S. J. et al. Fully automated chromatographic purification of Sr and Ca for isotopic analysis. *J. Anal. At. Spectrom.* **30**, 1906–1912 (2015).
243. Lamp, J. L. et al. Update on the cosmogenic in situ ^{14}C laboratory at the Lamont–Doherty Earth Observatory. *Nucl. Instrum. Methods Phys. Res. Sect. B Beam Interact. Mater. At.* **456**, 157–162 (2019).
244. Altenkirch, R. et al. Operating the 120° Dipol-Magnet at the CologneAMS in a gas-filled mode. *Nucl. Instrum. Methods Phys. Res. Sect. B Beam Interact. Mater. At.* **438**, 184–188 (2019).
245. Vockenhuber, C., Miltenberger, K.-U. & Synal, H.-A. ^{36}Cl measurements with a gas-filled magnet at 6 MV. *Nucl. Instrum. Methods Phys. Res. Sect. B Beam Interact. Mater. At.* **455**, 190–194 (2019).
246. Codilean, A. T. et al. Single-grain cosmogenic Ne-21 concentrations in fluvial sediments reveal spatially variable erosion rates. *Geology* **36**, 159–162 (2008).
247. McPhillips, D., Bierman, P. R. & Rood, D. H. Millennial-scale record of landslides in the Andes consistent with earthquake trigger. *Nat. Geosci.* **7**, 925–930 (2014).
248. Carretier, S., Regard, V., Leanni, L. & Farias, M. Long-term dispersion of river gravel in a canyon in the Atacama Desert, Central Andes, deduced from their Be-10 concentrations. *Sci. Rep.* **9**, 17763 (2019).
249. Muzikar, P. Episodic erosion with a power law probability density, and the accumulation of cosmogenic nuclides. *J. Geophys. Res. Earth Surf.* **124**, 2345–2355 (2019).
250. Skov, D. S., Egholm, D. L., Jansen, J. D., Sandiford, M. & Knudsen, M. F. Detecting landscape transience with in situ cosmogenic C-14 and Be-10. *Quat. Geochronol.* **54**, 101008 (2019).
251. Charreau, J. et al. Basinga: a cell-by-cell GIS toolbox for computing basin average scaling factors, cosmogenic production rates and denudation rates. *Earth Surf. Process. Landf.* **44**, 2349–2365 (2019).
252. Dannhaus, N., Wittmann, H., Kram, P., Christl, M. & von Blanckenburg, F. Catchment-wide weathering and erosion rates of mafic, ultramafic, and granitic rock from cosmogenic meteoric Be-10/Be-9 ratios. *Geochim. Cosmochim. Acta* **222**, 618–641 (2018).
253. Caesar, L., McCarthy, G. D., Thornalley, D. J. R., Cahill, N. & Rahmstorf, S. Current Atlantic meridional overturning circulation weakest in last millennium. *Nat. Geosci.* **14**, 118–120 (2021).
254. Chafik, L., Nilsen, J. E. Ø., Dangendorf, S., Reverdin, G. & Frederikse, T. North Atlantic Ocean circulation and decadal sea level change during the altimetry era. *Sci. Rep.* **9**, 1041 (2019).
255. Carter, B. R. et al. Pacific anthropogenic carbon between 1991 and 2017. *Glob. Biogeochem. Cycles* **33**, 597–617 (2019).
256. Ebser, S. et al. Ar-39 dating with small samples provides new key constraints on ocean ventilation. *Nat. Commun.* **9**, 5046 (2018).
257. Wang, J. S. et al. Optical excitation and trapping of Kr-81. *Phys. Rev. Lett.* **127**, 023201 (2021).
258. Yusoff, K. *A Billion Black Anthropocenes or None* (Univ. Minnesota Press, 2018).
259. Sahagun, L. Caltech says it regrets drilling holes in sacred Native American petroglyph site. *Los Angeles Times* https://www.latimes.com/environment/story/2021-07-19/caltech-fined-for-damaging-native-american-cultural-site (2021).
260. Bacon-Bercey, J. Statistics on Black meteorologists in six organizational units of the Federal Government. *Bull. Am. Meteorol. Soc.* **59**, 576–580 (1978).
261. Morris, V. R. Combating racism in the geosciences: reflections from a black professor. *AGU Adv.* **2**, e2020AV000358 (2021).
262. Ali, H. N. et al. An actionable anti-racism plan for geoscience organizations. *Nat. Commun.* **12**, 3794 (2021).
263. Hofstra, B. et al. The diversity–innovation paradox in science. *Proc. Natl Acad. Sci. USA* **117**, 9284 (2020).
264. Garcia, A. A., Semken, S. & Brandt, E. The construction of cultural consensus models to characterize ethnogeological knowledge. *Geoheritage* **12**, 59 (2020).
265. Handley, H. K. et al. In Australasia, gender is still on the agenda in geosciences. *Adv. Geosci.* **53**, 205–226 (2020).
266. Piccoli, F. & Guidobaldi, G. A report on gender diversity and equality in the geosciences: an analysis of the Swiss Geoscience Meetings from 2003 to 2019. *Swiss J. Geosci.* **114**, 1 (2021).
267. Stone, J. O. Air pressure and cosmogenic isotope production. *J. Geophys. Res.* **105**, 23753–23759 (2000).
268. Heisinger, B. et al. Production of selected cosmogenic radionuclides by muons: 2. Capture of negative muons. *Earth Planet. Sci. Lett.* **200**, 357–369 (2002).
269. Heisinger, B. et al. Production of selected cosmogenic radionuclides by muons; 1. Fast muons. *Earth Planet. Sci. Lett.* **200**, 345–355 (2002).
270. Dunai, T. J. & Lifton, N. A. The nuts and bolts of cosmogenic nuclide production. *Elements* **10**, 347–350 (2014).
271. Dunai, J. T. Cosmogenic nuclides: principles, concepts and applications in the earth surface sciences (Cambridge Univ. Press, 2010).
272. Bourles, D., Raisbeck, G. M. & Yiou, F. ^{10}Be and ^{9}Be in marine sediments and their potential for dating. *Geochim. Cosmochim. Acta* **53**, 443–452 (1989).
273. Pastuovic, Z. et al. SIRIUS — a new 6 MV accelerator system for IBA and AMS at ANSTO. *Nucl. Instrum. Methods Phys. Res. Sect. B Beam Interact. Mater. At.* **371**, 142–147 (2016).
274. Synal, H.-A., Stocker, M. & Suter, M. MICADAS: a new compact radiocarbon AMS system. *Nucl. Instrum. Methods Phys. Res. Sect. B Beam Interact. Mater. At.* **259**, 7–13 (2007).
275. Chen, C. Y. et al. Ultrasensitive isotope trace analyses with a magneto-optical trap. *Science* **286**, 1139–1141 (1999).
276. von Blanckenburg, F. & Willenbring, J. Cosmogenic nuclides: dates and rates of earth-surface change. *Elements* **10**, 341–346 (2014).
277. Granger, D. E. & Schaller, M. Cosmogenic nuclides and erosion at the watershed scale. *Elements* **10**, 369–373 (2014).
278. Dutton, A. et al. Sea-level rise due to polar ice-sheet mass loss during past warm periods. *Science* **349**, 153 (2015).
279. Melles, M. et al. 2.8 Million years of Arctic climate change from Lake El'gygytgyn, NE Russia. *Science* **337**, 315–320 (2012).
280. Funder, S. et al. A 10,000-year record of Arctic Ocean sea-ice variability — view from the beach. *Science* **333**, 747–750 (2011).
281. Fülöp, R. H., Wacker, L. & Dunai, T. J. Progress report on a novel in situ ^{14}C extraction scheme at the University of Cologne. *Nucl. Instrum. Methods Phys. Res. Sect. B Beam Interact. Mater. At.* **361**, 20–24 (2015).
282. Blard, P. H. et al. An inter-laboratory comparison of cosmogenic ^{3}He and radiogenic ^{4}He in the CRONUS-P pyroxene standard. *Quat. Geochronol.* **26**, 11–19 (2015).
283. Mechernich, S. et al. Carbonate and silicate intercomparison materials for cosmogenic Cl-36 measurements. *Nucl. Instrum. Methods Phys. Res. Sect. B Beam Interact. Mater. At.* **455**, 250–259 (2019).
284. Fraser, B. News in Focus: Daring scientists extract ice from Earth's highest tropical glacier. *Nature* **573**, 171–172 (2019).
285. North, M. A., Hastie, W. W. & Hoyer, L. Out of Africa: The underrepresentation of African authors in high-impact geoscience literature. *Earth Sci. Rev.* **208**, 103262 (2020).
286. Fiser, R., Lozier, S., Graumlich, L. & White, L. *AGU releases 2020 annual DEI report and new DEI dashboard* (American Geophysical Union, 2021).
287. Wadman, M. Disturbing allegations of sexual harassment in Antarctica leveled at noted scientist. *Science* https://doi.org/10.1126/science.aaq1428 (2017).
288. Crenshaw, K. Demarginalizing the intersection of race and sex: a black feminist critique of antidiscrimination doctrine, feminist theory, and antiracist politics. *Univ. Chic. Leg. Forum* **1**, 139–167 (1989).
289. Núñez, A.-M., Rivera, J. & Hallmark, T. Applying an intersectionality lens to expand equity in the geosciences. *J. Geosci. Educ.* **68**, 97–114 (2020).

Acknowledgements
J.M.S. acknowledges support by the National Science Foundation (NSF) (NSF-EAR-1933927) and the Vetlesen Foundation; J.K.W. acknowledges funding from grant NSF-EAR-1651243; A.T.C. and R.-H.F. acknowledge and pay respect to the traditional owners of the land on which they live and work; and Z.-T.L. acknowledges support from the National Natural Science Foundation of China (Grant No. 41727901). The authors are grateful to Y.-C. Fu for help in suggesting relevant references.

Author contributions
Introduction (J.M.S., A.T.C., J.K.W. and B.K.); Experimentation (J.M.S., A.T.C., J.K.W., Z.-T.L., R.-H.F. and B.K.); Results (J.M.S., A.T.C., J.K.W., Z.-T.L., R.-H.F., P.V. and B.K.); Applications (J.M.S., A.T.C., J.K.W., Z.-T. L., R.-H.F., P.V. and B.K.); Reproducibility and data deposition (J.M.S., A.T.C., J.K.W., P.V. and B.K.); Limitations and optimizations (J.M.S., A.T.C., J.K.W., Z.-T.L., R.-H.F. and B.K.); Outlook (J.M.S., A.T.C., J.K.W., Z.-T.L., R.-H.F., P.V. and B.K.); Overview of Primer (J.M.S. and J.K.W.).

Competing interests
The authors declare no competing interests.

Peer review information
Nature Reviews Methods Primers thanks Regis Braucher, Derek Fabel, Paula Hilger and the other, anonymous, reviewer(s) for their contribution to the peer review of this work.

Publisher's note
Springer Nature remains neutral with regard to jurisdictional claims in published maps and institutional affiliations.

RELATED LINKS
AGI Currents 2020: https://www.americangeosciences.org/sites/default/files/DB_2020-023-DiversityInTheGeosciences.pdf
ATTA method: http://atta.ustc.edu.cn/en-us/events/attaprimer.html
ExpAge: http://expage.github.io/
Froth flotation: https://www.physics.purdue.edu/primelab/MSL/froth_floatation.html
ICE-D: http://ice-d.org/
ICE-D production rate calibration data: http://calibration.ice-d.org/discussion/recent
IPCC SR15: https://www.ipcc.ch/sr15/
OCTOPUS: https://octopusdata.org/